NUSC Technical Report 7969
14 May 1987

Global Model for Sound Absorption in Sea Water Part III: Arctic Regions

R. H. Mellen
PSI - Marine Sciences

P. M. Scholfele
Combat Systems Analysis Staff

D. G. Browning
Surface Ship Sonar Department

Naval Underwater Systems Center
Newport, Rhode Island / New London, Connecticut

Preface

This report was prepared for the Naval Underwater Systems Center, Principal Investigator LT P. M. Scheifele (Code 61M). The report was prepared in large part by Dr. R. H. Mellen, Planning Systems Incorporated - Marine Sciences and co-authored by LT P. M. Scheifele, and D. G. Browning of the Naval Underwater Systems Center, New London Laboratory.

The authors wish to acknowledge T. Bell, B. Fisch, G. Smith, Dr. D. Klingbeil, J. Hanrahan, C. DeVoe, J. Doebler, and J. Dlubac for their guidance and assistance with the direction and format of the reports.

Reviewed and Approved: 14 May 1987

L. Freeman
Head, Surface Ship Sonar Department

J. Keil
Head, Combat Systems Analysis Staff

UNCLASSIFIED
SECURITY CLASSIFICATION OF THIS PAGE

REPORT DOCUMENTATION PAGE

1a. REPORT SECURITY CLASSIFICATION UNCLASSIFIED	1b. RESTRICTIVE MARKINGS
2a. SECURITY CLASSIFICATION AUTHORITY	3. DISTRIBUTION / AVAILABILITY OF REPORT Approved for public release; distribution is unlimited.
2b. DECLASSIFICATION / DOWNGRADING SCHEDULE	
4. PERFORMING ORGANIZATION REPORT NUMBER(S) TR 7969	5. MONITORING ORGANIZATION REPORT NUMBER(S)
6a. NAME OF PERFORMING ORGANIZATION Naval Underwater Systems Center 6b. OFFICE SYMBOL (If applicable) Code 61M	7a. NAME OF MONITORING ORGANIZATION
6c. ADDRESS (City, State, and ZIP Code). New London Laboratory New London, CT 06320	7b. ADDRESS (City, State, and ZIP Code)
8a. NAME OF FUNDING / SPONSORING ORGANIZATION 8b. OFFICE SYMBOL (If applicable)	9. PROCUREMENT INSTRUMENT IDENTIFICATION NUMBER
8c. ADDRESS (City, State, and ZIP Code)	10. SOURCE OF FUNDING NUMBERS PROGRAM ELEMENT NO. / PROJECT NO. / TASK NO. / WORK UNIT ACCESSION NO.

11. TITLE (Include Security Classification)
GLOBAL MODEL FOR SOUND ABSORPTION IN SEA WATER - PART III: ARCTIC REGIONS

12. PERSONAL AUTHOR(S)
R. H. Mellen (PSI), P. M. Scheifele and D. G. Browning (NUSC)

13a. TYPE OF REPORT	13b. TIME COVERED FROM ____ TO ____	14. DATE OF REPORT (Year, Month, Day)	15. PAGE COUNT
		1987 May 14	

16. SUPPLEMENTARY NOTATION

17 COSATI CODES			18. SUBJECT TERMS (Continue on reverse if necessary and identify by block number)
FIELD	GROUP	SUB-GROUP	

19. ABSTRACT (Continue on reverse if necessary and identify by block number)

Sound absorption in sea water is known to be caused by ionic relaxations involving magnesium sulfate, boric acid and magnesium carbonate. The mechanisms of the three relaxations have been determined by laboratory experiments and are now well-understood

Absorption is regionally dependent, due mainly to the pH-dependence of the boric acid relaxation. In the nominal sea-water pH range 7.7-8.3, the magnitude increases by roughly a factor of four at the lower frequencies. A 3-relaxation model has been developed from results of both laboratory and sea experiments. Predictions based on archival pH data have been found to be in good agreement with sound-channel measurements.

20. DISTRIBUTION / AVAILABILITY OF ABSTRACT ☐ UNCLASSIFIED/UNLIMITED ☒ SAME AS RPT ☐ OTIC USERS	21. ABSTRACT SECURITY CLASSIFICATION UNCLASSIFIED
22a. NAME OF RESPONSIBLE INDIVIDUAL P. M. Scheifele	22b. TELEPHONE (Include Area Code) (203) 440-6589 22c. OFFICE SYMBOL Code 61M

DD FORM 1473, 84 MAR 83 APR edition may be used until exhausted. All other editions are obsolete.

SECURITY CLASSIFICATION OF THIS PAGE
UNCLASSIFIED

19. ABSTRACT (Cont'd.)

Since pH varies with depth as well as location, absorption also depends on the ray paths. A predictive global model for the World Ocean has been developed, employing contour charts of the pH correction-factor (K-factor) at the depths 0, 0.5, 1, 2, and 4 km. Profiles required for loss-integration along ray paths can be generated by the algorithm provided. This report extends

The purpose of this report is to extend the model to cover Arctic regions. In polar waters, sound speed generally increases monotonically with depth and upward refraction causes a concentration of energy near the surface. Excess attenuation, evidently due to underice scattering, makes long-range propagation feasible only at very low frequencies. Reverberation is also an thus order of magnitude higher than that at lower latitudes. Absorption effects are then important only for direct-paths and high frequencies. For depths of 1 km or less, the ranges of concern are therefore no greater than about 50 km in ice-covered waters.

The range of pH in the Arctic Ocean is roughly 8.0-8.3, corresponding to an absorption range of a factor of two at most. Because the variability occurs much closer to the surface, the depths 0, 0.1, 0.3, 0.5 and 1 km have been selected for the K-contour charts. Depths greater than 1 km are found only in basin regions and variability is negligible at these depths.

The proposed method for predicting sound absorption in Arctic regions appears to satisfy accuracy requirements.

Table of contents page

Introduction

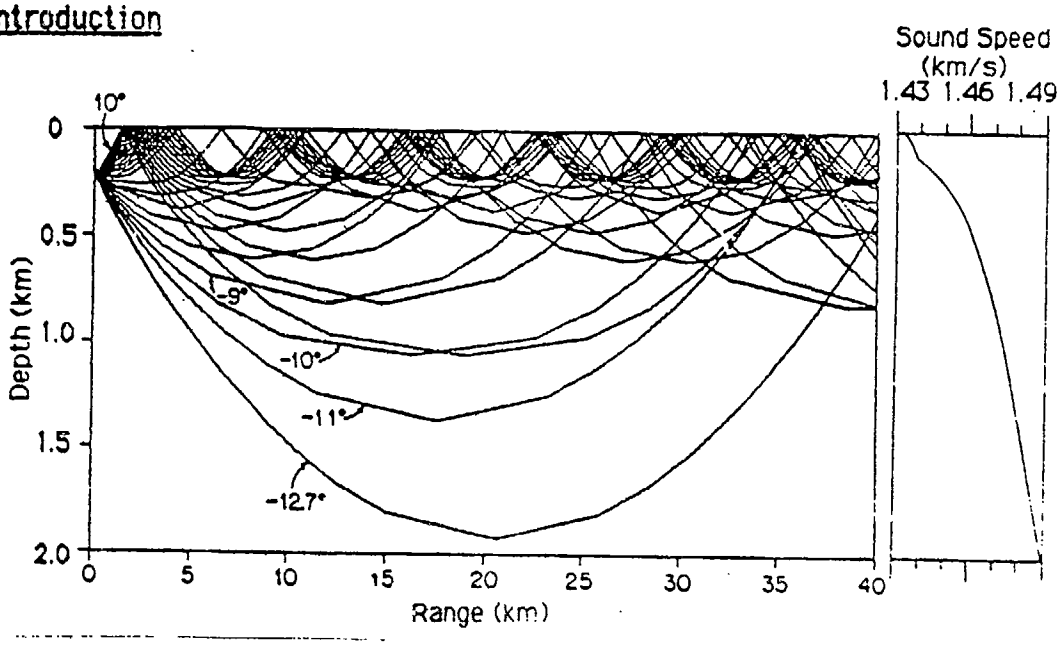

Figure 1: Arctic Ocean sound-speed profile and ray diagram.

The Arctic Ocean is a unique acoustic environment, principally because the sound speed increases monotonically with depth and the surface is generally covered by an ice layer. Upward refraction and scattering at the rough ice-water interface produce reverberation and attenuation, both of which place severe limitations on SONAR performance.

Figure 1 shows a typical sound-speed profile and ray diagram. In deeper waters, the maximum RSR cycle distance can be of the order of 50 km. In this range, reverberation and absorption in the medium can be the most important factors. At longer ranges, most of the energy is concentrated in rays with small grazing angles and multiple reflections at the ice-water interface are then involved. Scattering causes losses in both energy and signal coherence and these losses can exceed absorption loss by more than an order of magnitude.

The main purpose of this report is to extend the current global-model for sound absorption in sea water [1,2] to include Arctic regions. The model is based on the three principal chemical relaxations contributing to sound absorption. An approximate formula has been developed and predictions compared favorably with experimental data from many parts of the World Ocean. The environmental factors involved in absorption prediction are pH and temperature. Investigation of the effects of pH on propagation loss will be a principal concern. However, reverberation and attenuation due to scattering will also be addressed because of their great importance in the overall problem.

Background

By the end of WWII, it was known that absorption at SONAR frequencies is more than order of magnitude greater in sea water than in fresh water. Subsequent propagation experiments provided accurate estimates of the magnitude. By the early 1950's, laboratory resonator experiments had identified the cause as a magnesium sulfate relaxation and details of the mechanism and the relaxation parameters had been worked out. In 1962, Schulkin and Marsh [3] proposed a formula for sea-water absorption, based on both the measured relaxation parameters and field experiments in the frequency range 2-30 kHz.

In 1965, Thorp [4] reported sound-channel propagation experiments in the Bermuda-Eleuthera area indicating an anomaly at lower frequencies. The extra loss was fitted by adding a 1 kHz relaxation to the S&M formula and the result became known as the "Thorp formula" [5].

Mediterranean experiments were reported by Leroy [6], showing a similar anomaly but with somewhat higher magnitude and relaxation frequency. Experiments carried over the next two decades in other areas confirmed the high degree of variability of the extra loss and regional dependence has therefore become much more critical [7]. The major factor involved in this variability has been identified as the pH value [8].

The principal chemical relaxation responsible for the pH-dependent loss has been shown to involve boric acid [9]. The chemical mechanism has been identified as the boric acid/carbonate equilibrium and the parameters have been measured in the laboratory by means of the resonator method [10]. The laboratory investigations also revealed a pH-dependent relaxation involving magnesium carbonate, which has been found to play a minor but significant role in sea water absorption [11].

An absorption formula, based solely on known chemical processes, would be far too complex and the accuracy would be limited as well. However, since the range of environmental parameters in the World Ocean is very limited, simplifying approximations can be made; namely, that the losses for both pH-dependent relaxations increase exponentially with pH and the relaxation frequencies increase exponentially with temperature. Thorp's formula can then simply be modified by adding the third relaxation and including the required pH and temperature corrections.

A 3-relaxation formula has already been developed. Predictions based on archival pH data have been tested against all the available sound-channel with good results [1,12].

Absorption Model

$$A = A_1(MgSO_4) + A_2(B(OH)_3) + A_3(MgCO_3)$$

$$A_n = (S/35)\, a_n f^2 f_n / (f^2 + f_n^2)$$

$$a_1 = 0.5 \times 10^{-D(km)/20} \qquad f_1 = 50 \times 10^{T/60}$$

$$a_2 = 0.1 \times 10^{(pH-8)} \qquad f_2 = 0.9 \times 10^{T/70}$$

$$a_3 = 0.03 \times 10^{(pH-8)} \qquad f_3 = 4.5 \times 10^{T/30}$$

Atlantic 4°C pH 8.0
$A = 0.007f^2 + 0.1\, f^2/(1+f^2) + 0.18\, f^2/(6^2+f^2)$
N.Pacific 4°C pH 7.7
$A = 0.007f^2 + 0.05f^2/(1+f^2) + 0.09\, f^2/(6^2+f^2)$
Mediterranean 14°C pH 8.3
$A = 0.006f^2 + 0.26f^2/(1.4^2+f^2) + 0.78\, f^2/(12^2+f^2)$
Red Sea 22°C pH 8.2
$A = 0.004f^2 + 0.27f^2/(1.8^2+f^2) + 1.1f^2/(24^2+f^2)$
sub-Arctic -1°C pH 8.3
$A = 0.01f^2 + 0.17\, f^2/(0.85^2+f^2) + 0.24\, f^2/(4^2+f^2)$

Figure 2: Simplified absorption formulae.

In the 3-relaxation formula of Figure 2, A is in dB/km, frequency f and relaxation frequencies f_n are in kHz, temperature T is in °C and pH=8.0 the reference value. PH values in the World Ocean very roughly from 7.7 to 8.3, which corresponds to an absorption ratio of as much as 4/1 at the lower frequencies.

The magnesium sulfate term includes the depth factor D(km), which is adapted from the pressure correction of Fisher and Simmons [13]. Depth dependencies of the other two relaxations are not yet known; however, measurements in both deep and shallow channels indicate that boric acid effects are negligible. Magnesium carbonate effects may be greater but can be neglected because its contribution is so small. Salinity dependence has been approximated as S/35 where S is parts per thousand.

Specific coefficients for several experimental areas, are shown in the bottom box. Note that the magnesium sulfate terms are approximations valid only for frequencies less than 10 kHz.

Model and data comparison

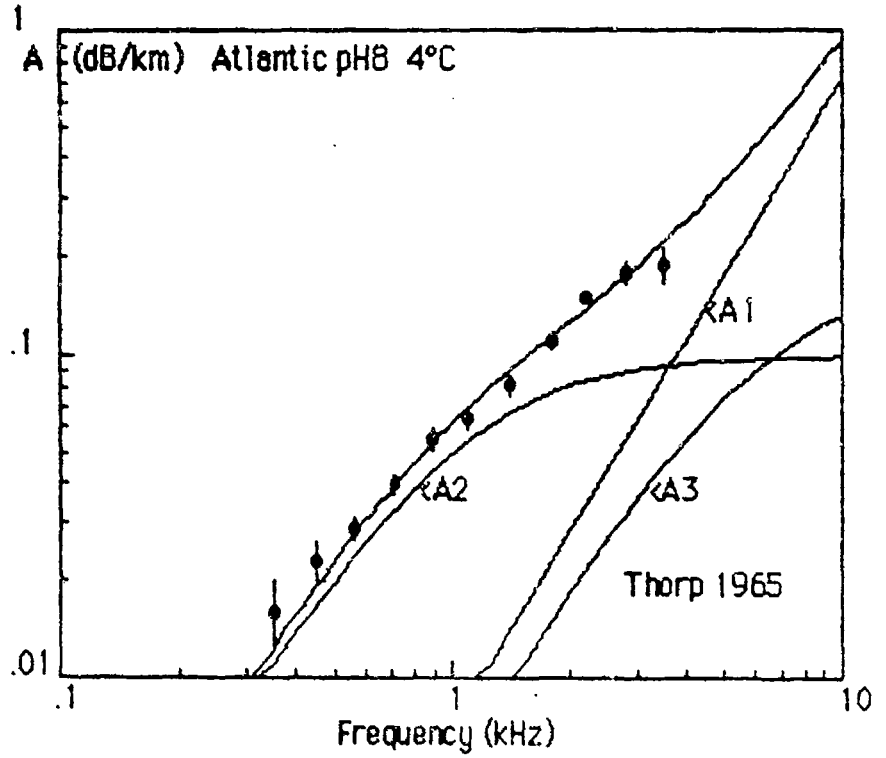

Figure 3: Thorp's data and 3-relaxation model.

Figure 3 compares Thorp's data with the 3-relaxation model. Individual components are identified and the top curve is their sum. The overall fit to the data with the new model is as good or better than that with the Thorp formula: $A = 40f^2/(4100+f^2) + 0.1f^2/(1+f^2)$ dB/kyd.

Note that the A2 (boric acid) coefficient is 10% lower than that of the second term in the Thorp formula; i.e. the value in dB/km becomes equal to the Thorp value in dB/kyd. The differences in total absorption at the lower frequencies are made up by the A3 (magnesium carbonate) component.

The parameter adjustment is mainly justified on the basis of data-fit, the third component being essential to the model. When the sea-water resonator data were fitted with a 2-relaxation model, there were serious discrepencies at higher pH values. For example, at pH=8.5, formula values that were too low by a factor of more than two at the lower frequencies, which was clear evidence of the existence of a third component. Sea water synthesis experiments were carried out and the mechanism was identified as the magnesium-carbonate relaxation. The relaxation parameters and the temperature and pH dependencies were determined by measurement.

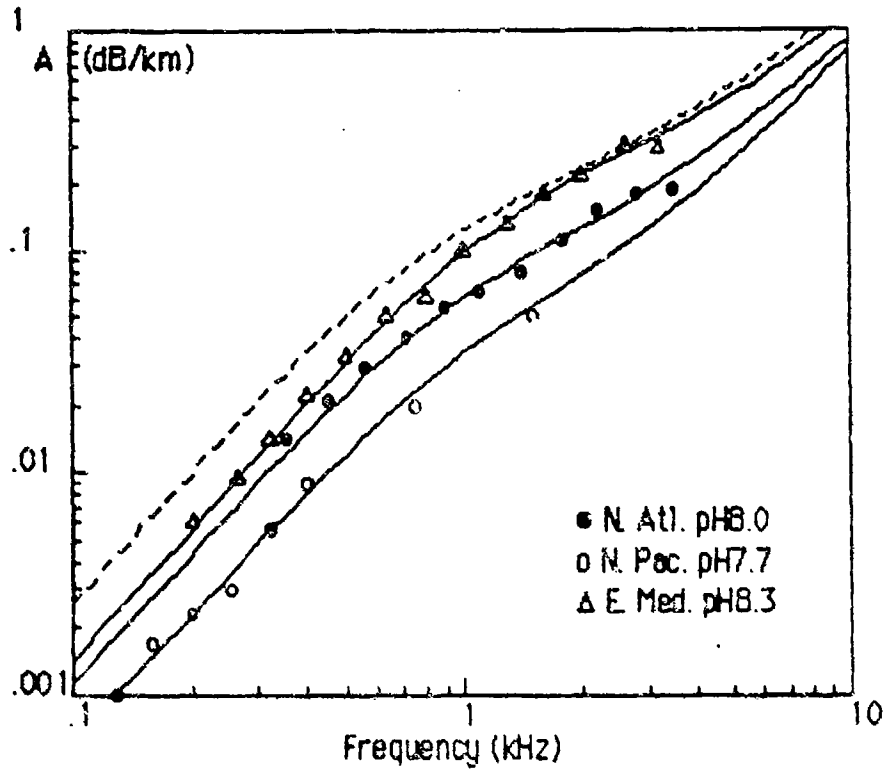

Figure 4: Model and data comparison.

Figure 4 compares the 3-relaxation model predictions with data from sound-channel experiments in the North Atlantic (Thorp), North Pacific, Mediterranean Sea and estimates for the Arctic (dashed curve).

In the North Pacific case [14], the lower value pH=7.7 reduces both the boric acid (A2) and the magnesium carbonate (A3) coefficients by a factor of two compared to the N. Atlantic. Relaxation frequencies depend only on temperature and remain the same.

In the Mediterranean case [15], the higher value pH=8.3 increases both the boric acid (A2) and the magnesium carbonate (A3) coefficients by a factor of two compared to the N. Atlantic. The curves do not differ by such a large factor at the lower frequencies because the relaxation frequencies are higher. The effect of lower relaxation frequencies in the Arctic, for the same value pH=8.3, is shown by the dashed curve.

The value pH=8.0 has been assumed for Thorp's experiment and is used as reference value in the 3-relaxation model. Predictions, based on archival pH values, show good agreement within experimental limits for all regions of the World Ocean examined. However, small adjustments of parameters can be made if new absorption and/or pH data indicate the need.

Details of the model in the Arctic regions will be considered next.

Figure 5. Arctic Ocean features

Figure 5 shows the general features of the Arctic Ocean. Depths greater than 3 km occur in only five main regions; namely, the Canadian, Makarov, Fram, Nansen and Norwegian basins. In these regions, good propagation via the half-channel can be expected to very long ranges. Spreading loss is then cylindrical, however, scattering losses limit useable frequencies to less than 100 Hz for ranges much greater than 100 km.

The basins are separated by the various ridges, the most prominent being the Lomonosov, which runs through the pole. Surrounding the deep basins are the shelf regions, in which the depths rapidly decrease to less than 500 m. In the shallower waters, the bottom can cause even higher losses because the deeper-going rays are cut off.

Arctic Attenuation

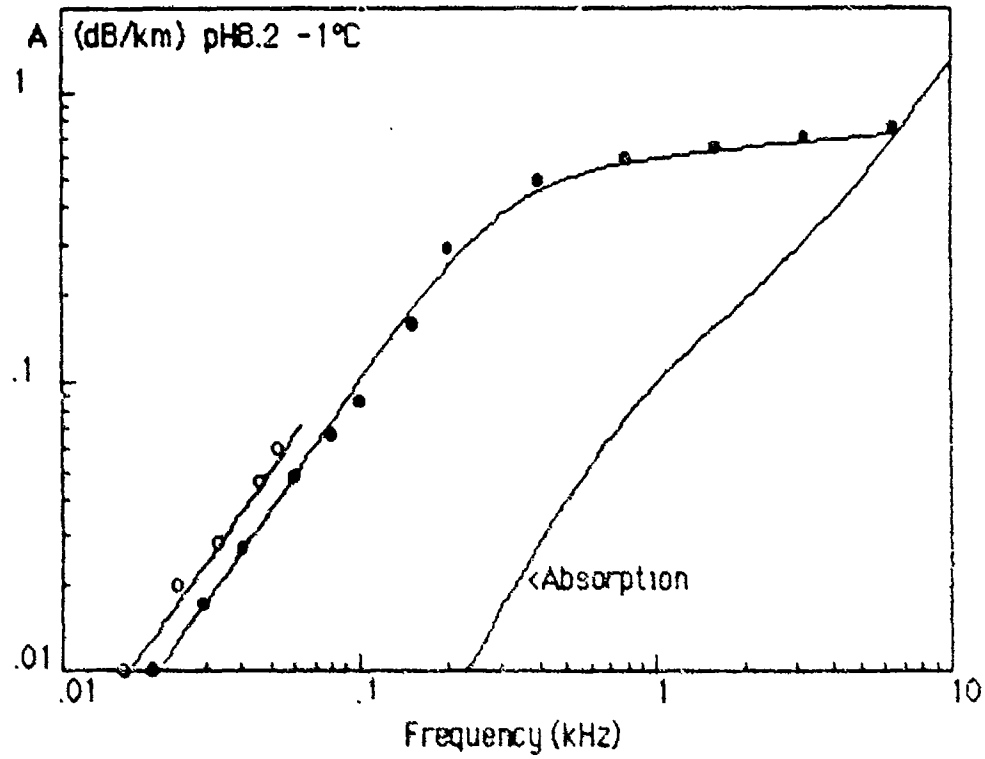

Figure 6. Arctic attenuation measurements.

Figure 6 compares measured attenuation data with estimated absorption for central Arctic waters. The solid circles are 1959 data [16] and open circles are Tristen/Fram-82 data [17]

The striking features of the data are the magnitude and resemblence to relaxational absorption. In the low-frequency range, values are more than 10 times greater than predicted absorption The relaxation-like behavior is believed due to experimental conditions. Attenuation usually limits the useable range to less than 100 km at higher frequencies and absorption dominates in this régime. Smaller losses at low frequencies require much longer ranges for measurement and scattering then becomes dominent

The likely low-frequency loss mechanism is scattering at the ice-water interface. Scattering theory shows that loss-per-bounce depends almost linearly on grazing angle. Since the skip distance has roughly the same dependence, loss-vs-range tends to depend more on gradient than angle for grazing angles less than about 6°

Larger-angle rays encounter a much smaller gradient, however, initial divergence-loss is greater and they tend to contribute little at the longer ranges Cutoff by the bottom may be an important factor

Ice Model

The first attempts to model underice scattering were based on the theory of Marsh [18]. The Marsh formula for forward-scatter loss employed the Neumann-Pierson sea-surface spectrum and the assumption was made that the ice-water interface acts like a pressure-release surface.

The theory appeared to give plausible results; i.e. values consistent with experiment were predicted for the RMS standard deviation 2.4 m for the underice roughness. This value was in fair agreement with measurements of underice profiles by upward-looking SSN sonar.

The approximations in Marsh theory make it valid over a limited range of frequencies and grazing angles. Recent advances in scattering theory by Brekhovskikh & Lysanov [19] now permit calculation of forward-scatter loss for all angles and frequencies. To carry out the necessary numerical calculations, it is convenient to have an analytic statistical model of the underice-roughness.

In the Tristen/Fram-82 experiment [17], underice profiles were obtained concurrently with the propagation measurements. Profile data for 400 km range were analyzed in 1 km segments and averages were taken over ten contiguous segments. The power spectra, correlation functions and PDF's (probability-density function) of draft were calculated by the FFT method. Standard deviations were derived from the PDF's and correlation lengths were estimated by fitting with the model correlation function.

Average values of correlation length and RMS standard deviation were found to be 44m and 2m, respectively, and the scatter of the 10 km data was reasonably uniform. Correlation between standard deviation and draft was quite high; however plots of correlation length vs standard deviation showed considerable scatter.

Figure 7 is a sketch of a small segment of an underice profile. The power spectrum shows typical FFT data and the curve-fit with the 1-dimensional analytic spectrum. The correlation function R(r) and the 2-dimensional spectrum have been derived analytically from the 1-dimensional spectrum. The angular-distribution of R(r) has been taken to be effectively isotropic and K_1 is the modified Bessel function.

The statistical parameters are correlation length and standard deviation The original theory of Marsh required only standard deviation because the correlation length is implicit in the Neumann-Pierson spectrum.

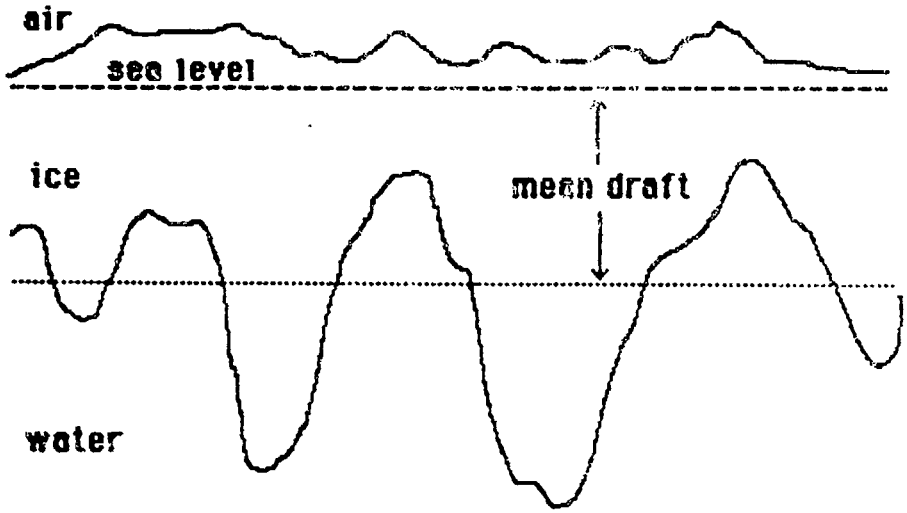

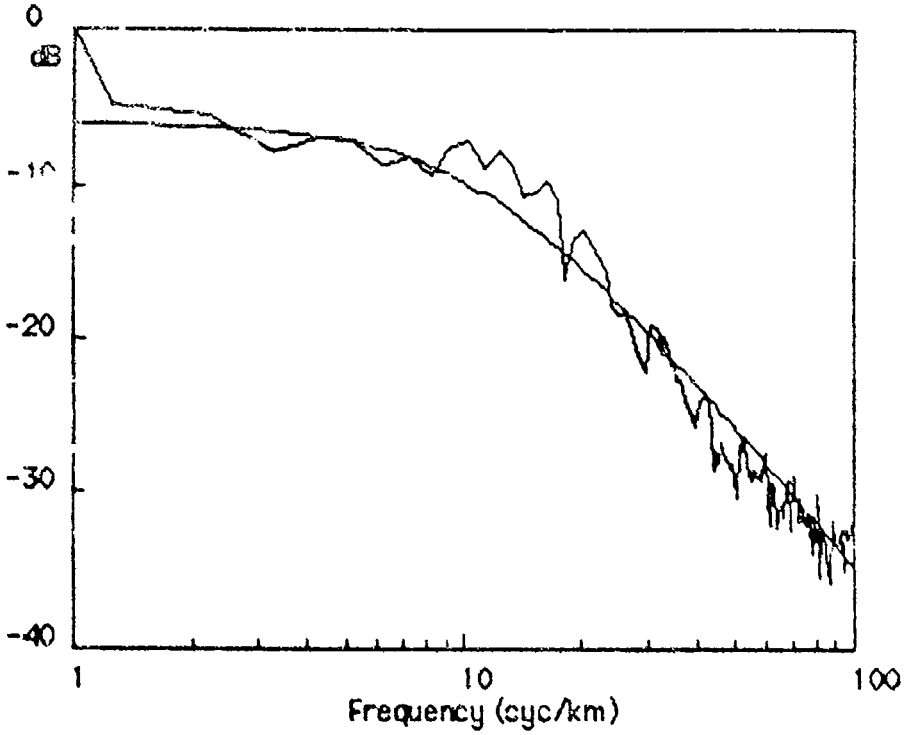

1-Dimensional Spectrum $S_1 = h^2 \Omega_0^2 (\Omega_0^2 + \Omega^2)^{-3/2}$
Correlation Function $R = \Omega_0 r K_1(\Omega_0 r)$
2-Dimensional Spectrum $S_2 = 2 h^2 \Omega_0^2 (\Omega_0^2 + \Omega^2)^{-2}$
Standard Deviation RMS $h = 2m$
Correlation Length $L = 2/\Omega_0 = 44m$

Figure 7: Ice roughness spectrum model.

Scattering-loss theory

The reflection coefficient Q is taken here as the ratio of the coherent signal-intensity in the specular direction to the incident intensity. In the perturbation approximation we let Q=1-SL where SL<<1. By removing the Neumann-Pierson spectrum from the Marsh formula, his result becomes $SL=3.3\ k^{3/2}\ L^{-1/2}\ h^2 \sin\theta$, where θ is the grazing angle, $k=2\pi f/C$ is acoustic wavenumber and C is the sound-speed.

The ray skip-range is given by $R(\theta)=2C\tan\theta/g$. Loss vs range is therefore almost independent of ray-angle for constant gradient g. Taking g=.06/sec. (near the surface) and the values h=2m, L=44m, the attenuation coefficient becomes $A=4.34\ SL/R(\theta) \approx 1.5\ f^{3/2}$ dB/km, where f is in kHz.

This approximation gives good agreement with the data trend of Figure 6 but it is low by roughly a factor of two. The discrepency is due mainly to the lower value of rms roughness. More exact computation, using computer codes for estimating propagation loss and adding the calculated reflection loss-per-bounce, gives comparable results.

The Marsh formula is valid only over a limited domain. Since it involves correlation length, the scatter beam-pattern is clearly involved. A general theory for all domains is given by equation 9.6.3 of B&L, which is a double integral over the surface-roughness spectrum.

In this paper, the B&L integral is transformed into scatter-angle space to show where the energy goes. For the analytic ice spectrum, the problem then reduces to a single integral to be evaluated numerically. Evaluation of the B&L double-integral gives identical results.

Asymptotic solutions of the integral are also obtained, which show the following limiting conditions:

In the Eckart régime [20], the scattered energy tends toward specular and the losses go as f^2. Values then become higher than the Marsh formula; however, the method of small perturbations (MSP) requires the condition $kh \sin\theta << 1$, which is violated at the higher frequencies.

In the Marsh régime, the losses go as $f^{3/2}$ and the scattering beamwidth becomes important. Some energy will then escape and be absorbed in the bottom, which could explain why there is no evidence of incoherent energy at longer ranges.

In the Rayleigh régime, scattering becomes diffuse and losses go as f^4. For the correlation length 44m, low-frequency roll-off can be expected below about 50 Hz and losses will then be less than the Marsh formula.

The results are summarized in the following equations:

Coherent Energy Reflectivity Q=1-SL

$$SL=(2\pi)^{-1}k^4h^2\sin\theta\int_0^{\pi/2}d\theta'\sin^2\theta'\cos\theta'\int_{-\pi}^{\pi}d\phi\int_0^{\infty}rdrR(r)J_0(k'r)$$

$$k'=k(\cos^2\theta+\cos^2\theta'-2\cos\phi\cos\theta\cos\theta')^{1/2}$$

$$k=2\pi f/C \qquad R(r)=\Omega_0 r\,K_1(\Omega_0 r)$$

$$k^2\int_0^{\infty}rdrR(r)J_0(k'r)=2(1+(k'/\Omega_0)^2)^{-2}\equiv F_1$$

First Integral

$$(2\pi)^{-1}\int_{-\pi}^{\pi}d\phi F_1=(1+u^2)((1+u)^2-v^2)^{-3/2}\equiv F_2$$

$$u=(k/\Omega_0)^2(\cos^2\theta+\cos^2\theta') \quad v=2(k/\Omega_0)^2\cos\theta\cos\theta'$$

Second Integral

$$SL=(kh)^2\sin\theta\int_0^{\pi/2}d\theta'\sin^2\theta'\cos\theta'F_2$$

Final integral to evaluate numerically

Eckart	$SL=(2kh\sin\theta)^2$	$Ru\gg1$ $kL\gg1$
Marsh	$SL=3.3(kh)^2\sin\theta(kL)^{-1/2}$	$Ru\ll1$ $kL\gg1$
Rayleigh	$SL=2(kh)^2(kL)^2\sin\theta/3$	$kL\ll1$
	$L=2/\Omega_0$ $Ru=kL\sin^2(\theta/2)$	

Asymptotic Approximations

The theory is based on Bragg-scattering wherein k' defines a matching between the acoustic (k) and the surface (Ω) wavenumbers as a function of the incident (θ) and scatter (θ') grazing angles.

The first integral over radius r yields an analytic function involving the ratio k'/Ω_0. (J_0 is the Bessel function.)

The second integral over azimuthal angle ϕ is also analytic, leaving only an integral over scatter angle θ' to evaluate numerically. The asymptotic solutions provide a check. (Parameter Ru refers to Rutherford-scattering.)

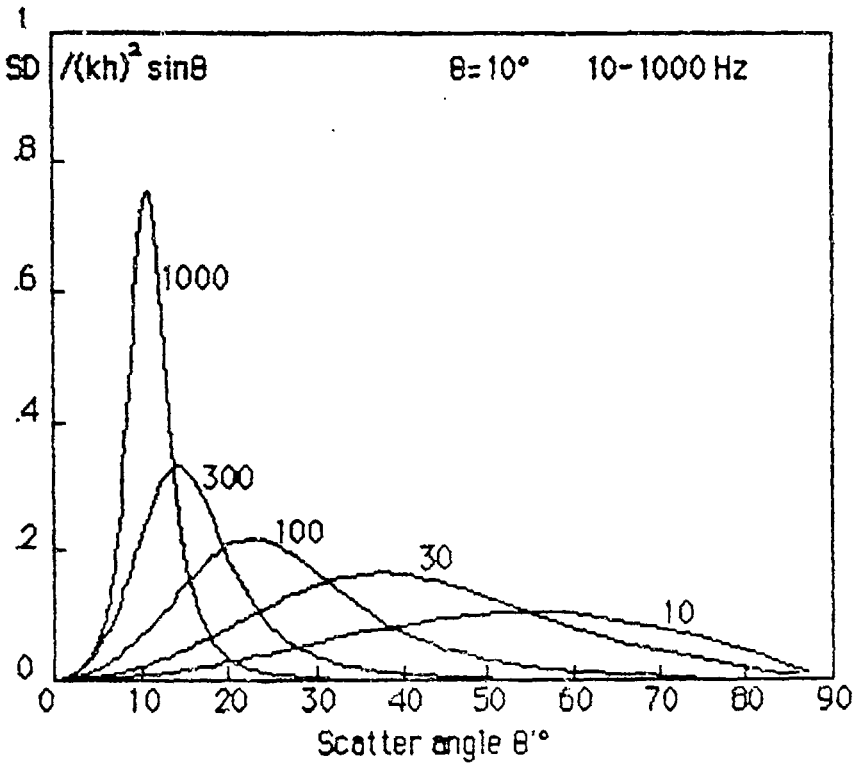

Figure 8: Ice spectrum integrands vs scatter angle.

Integrands of the scattering-loss equation are a measure of scattering directivity. Figure 8 show plots of amplitude vs scattering grazing-angle for an incident grazing angle $\theta=10°$. The curves have been normalized by dividing by $(kh)^2\sin\theta$ in order to restrict the range. At low frequencies, the scattering becomes diffuse in the half-space, while, at high frequencies, it tends to become specular.

The integrands can be considered as the energy scattered from an area of radius equal to the correlation length. It is therefore coherent with the incident plane-wave. Summing over a random ensemble of areas makes the result incoherent.

The integrands are similar to conventional beam-patterns; however, they are a measure of the flux in a cone and are not the usual cross-sections. The fraction of scattered energy remaining in the refractive régime can be readily estimated from the curves. For example, if 15° rays hit the bottom, more than 1/2 can be lost for each surface- reflection at frequencies less than 1 kHz. After several reflections, the incoherent levels will converge rapidly and become negligible.

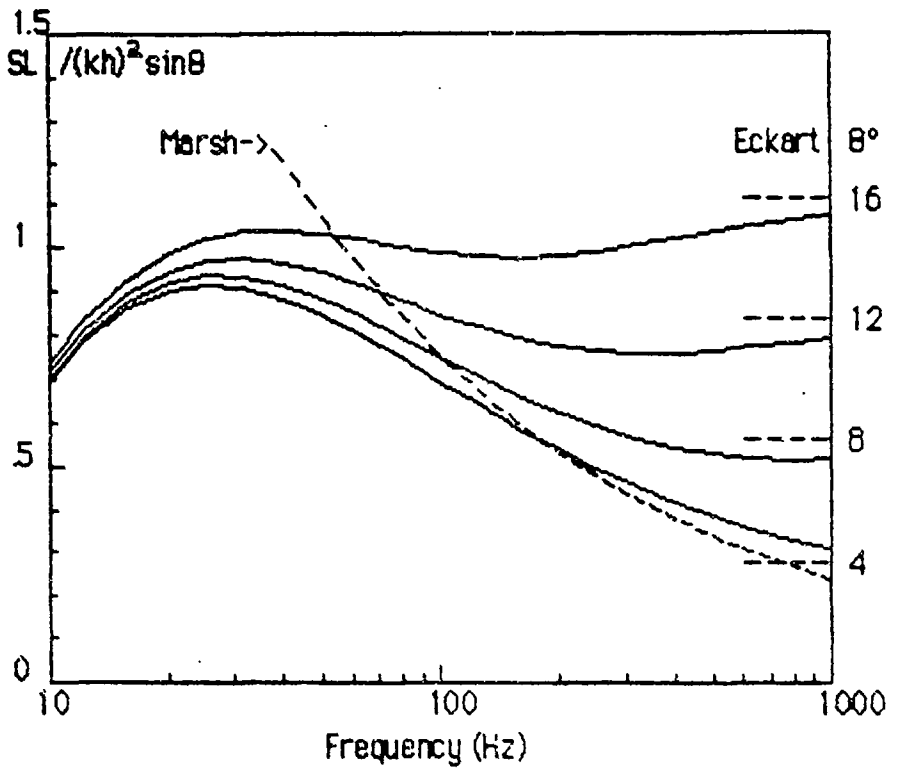

Figure 9: Ice spectrum scattering coefficients vs frequency.

In Figure 9, values of the integral obtained by numerical integration are plotted as a function of frequency for grazing angles 4-16°, which is the range of interest. Note that the curves have been normalized by dividing the scatter-loss by $(kh)^2\sin\theta$. This makes the Marsh formula (dashed line) and the Rayleigh low-frequency asymptote independent of angle while the Eckart high-frequency asymptotes become proportional to $\sin\theta$. The Marsh formula becomes inaccurate at the lower frequencies where the Rayleigh limit becomes important and also at the higher frequencies where the Eckart limit becomes important.

Loss estimates below 100 Hz by the Marsh approximation have already proven low by more than a factor of 2. The values obtained by integration become even smaller at low frequencies. Since the conditions for the MSP theory are apparently valid in this range, the cause of disagreement is not clear. The values do increase in the Eckart régime, but the MSP conditions rapidly become invalid here.

One possible additional loss mechanism is dissipation within the ice; however, very high backscatter levels are also observed and this suggests that there is more scattering than can be accounted for.

Attenuation summary

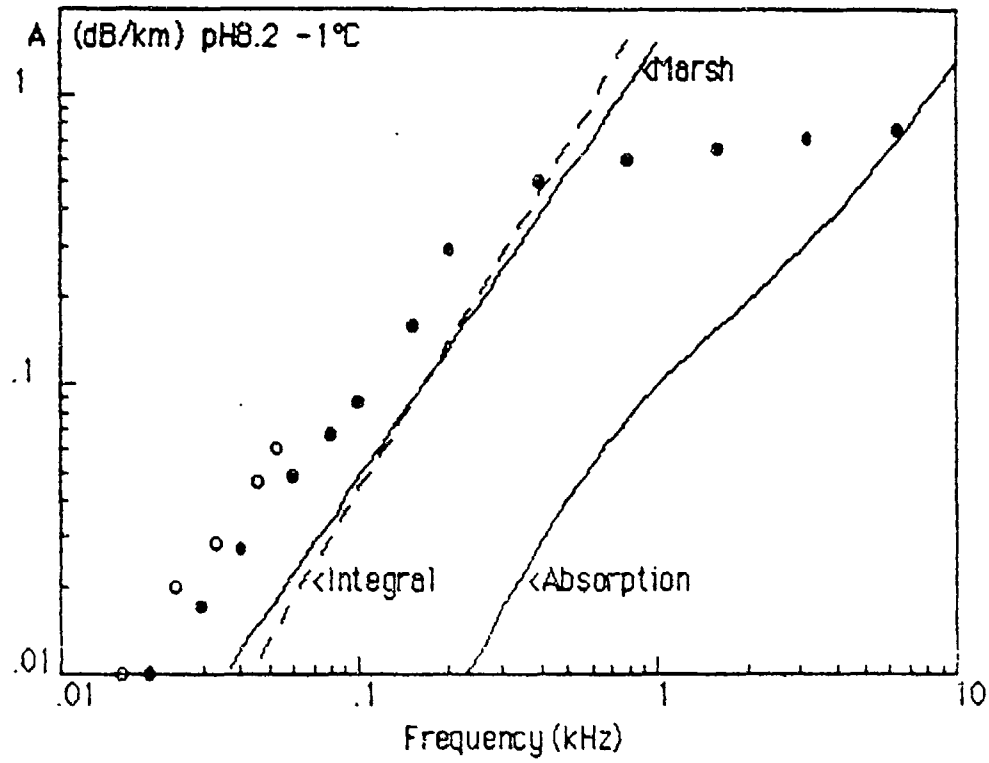

Figure 10: Attenuation vs frequency models.

The attenuation results are summarized in Figure 10, showing the two scattering models and the experimental data.

The solid curve on the left is the Marsh formula in which scattering loss increases as $f^{3/2}$. Predictions are low by more than a factor of two at the lower frequencies.

The dashed curve is the numerical-integration model covering all three regimes. The roll-off below 100 Hz indicates a gradual transition to the Rayleigh regime in which scattering becomes diffuse and scattering loss approaches an f^4 asymptote. The increase in magnitude above 200 Hz is the transition to the specular Eckart-regime where the asymptote is f^2.

Clearly, the more general scattering model and more accurate knowledge of the underice statistics has not improved agreement between experiment and theory. Without the pressure-release assumption for the ice-water interface, finite impedance effects would cause the magnitudes to fall off even more rapidly below 200 Hz. Air trapped near the bottom of the ice is a possible mechanism for effectively zero impedance; however, further experiments are required for verification. Even with this assumption, the agreement with data is still far from satisfactory.

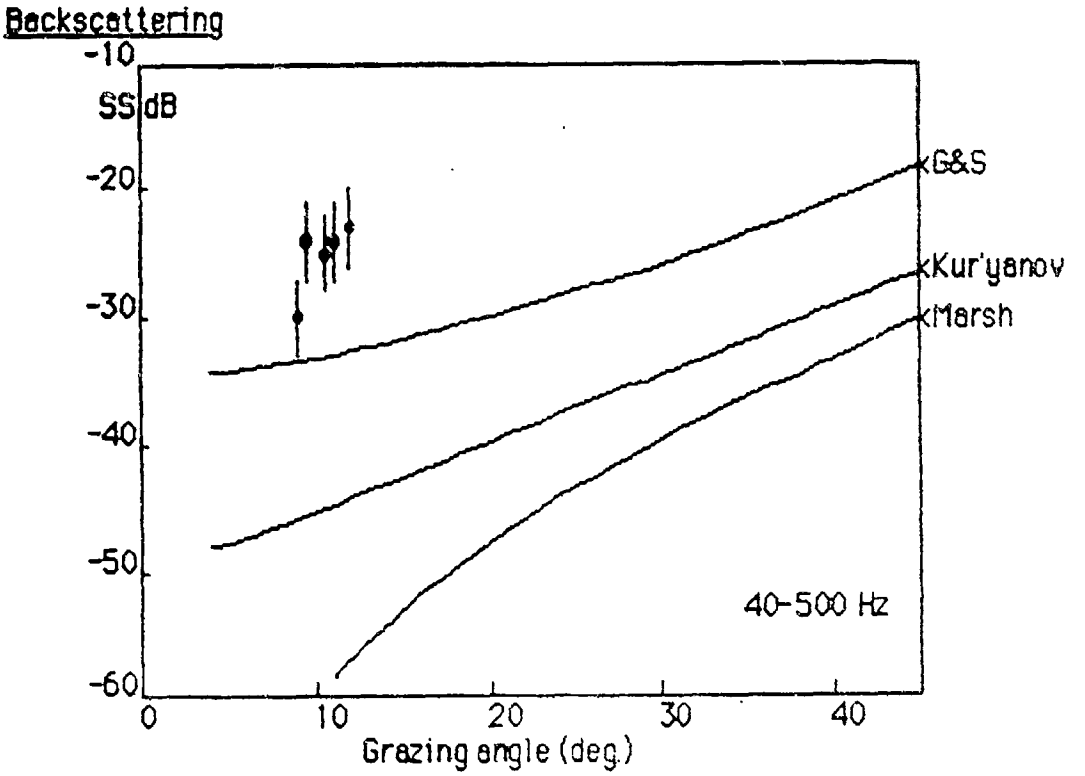

Figure 11: Backscatter strength vs grazing angle.

From the theory of Marsh [21], the ratio of the scattered to the incident intensity is proportional to $k^4 \sin^2\theta\ S_2(\Omega)$, where $\Omega=k'$ and k' is the Bragg wavenumber For backscattering, $\theta'=-\theta$ and the backscattering strength is:

$SS(dB)= 40 \log(\sin\theta) + 10 \log[k^4 S_2(\Omega)]$ $\quad \Omega\approx 2k \cos\theta$

Since the strength goes as k^4 and the spectrum goes asymptotically as Ω^{-4}, the result is independent of frequency above about 50 Hz and is simply:

$SS(dB)\approx -30 + 40 \log(\tan\theta)$

The data points in Figure 11 are average values for the band 40-500 Hz. The grazing angles are all close to 10° and no trend is obvious for such a limited range.

The Marsh formula prediction falls well below the data. The two-scale model of Kur'yanov [22] attempts to account for the effects of finite slope by assuming that the scatterers are small in scale compared to the scale of the gross roughness. The model of Greene and Stokes [23] assumes that the slope distribution of the gross roughness is non-Gaussian and that the backscattering is dominated by regions of highest slope, i.e. at pressure ridges. Curve "G&S" shows the prediction for the slope value 30°.

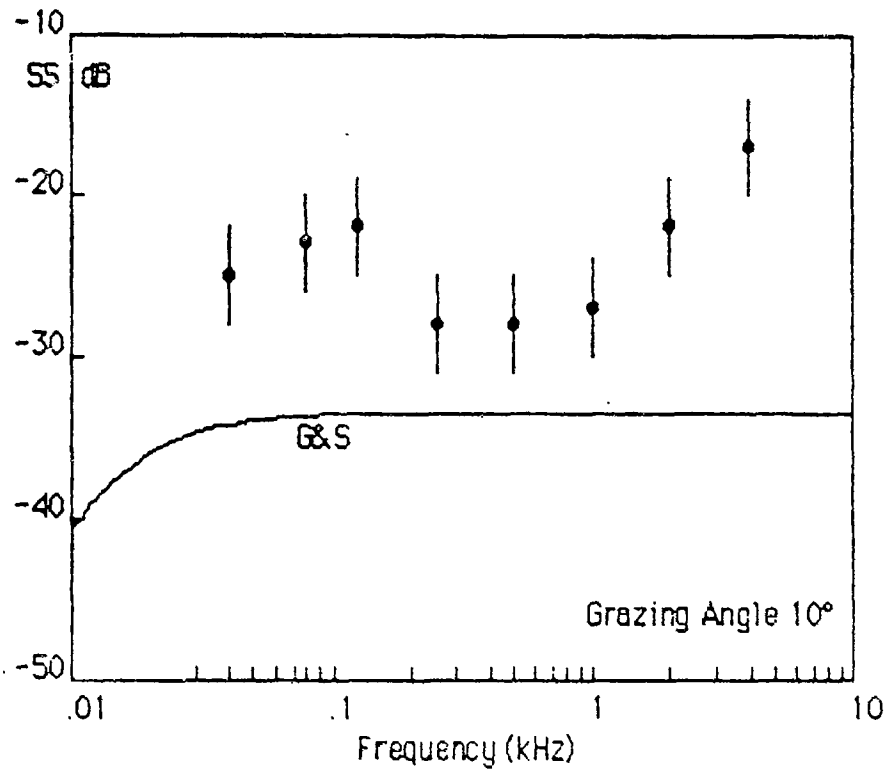

Figure 12: Backscatter strength vs frequency.

Figure 12 shows the backscattering data vs frequency for grazing angles near 10°. The "G&S" prediction falls off below 50 Hz because the acoustic wavelength becomes greater than the horizontal scale of roughness.

Finite impedance at the ice-water interface could also have significant effect at low frequencies here; i.e. if the impedance discontinuity begins to disappear below 200 Hz, scattering in any direction will rapidly become negligible. Therefore, without the pressure-release assumption, matters would be even worse.

It is clear that surface backscatter-strengths in ice-covered regions are extremely high. It is also clear that the theoretical models for both the backscattering strength and forward-scattering loss are not in adequate agreement with experiment, even with the pressure-release assumption and composite-roughness models.

The only logical conclusion appears to be that the scattering theory is at fault. Further theoretical investigations are obviously needed to see if a model can be developed that accounts for the observed magnitudes. Effects of the ice impedance must be included and this could require experiments to determine the pertinent physical properties.

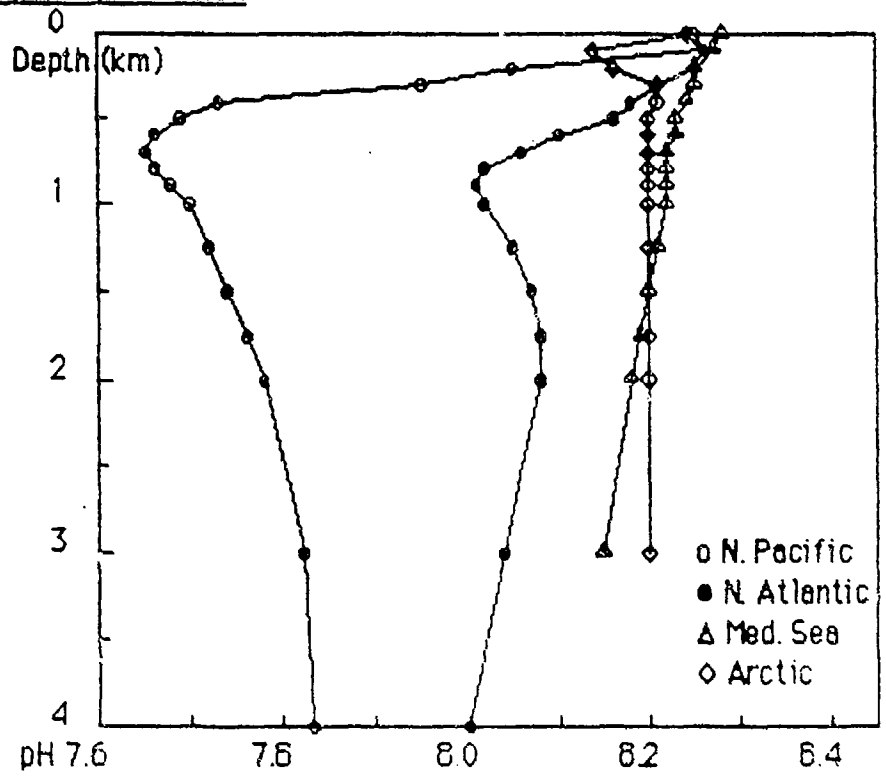

Figure 13: Comparison of pH profiles.

Figure 13 compares an Arctic pH profile with the extreme cases in the lower latitudes. Although the pH values tend to be fairly high, it is clear that sound absorption has a far less important role in the Arctic because the excess attenuation is so great

In earlier reports [1,2], the problem of pH variability and prediction of its effects on absorption was addressed. From analysis of propagation data from the lower latitudes, it was shown that one method of estimating the depth variations is to use selected depth-values for various propagation modes; i.e. axial values for sound channels, surface values for surface ducts and 2 km values for convergence zones.

Contours of pH for the surface and for depths 0.5 km and 1 km from the World Ocean Atlas Vol. 1 [24] were used together with contours for 2 km depth from Vol. 2 in developing appropriate charts for the three modes of propagation. Since the Russian pH contour intervals are large (0.1 pH unit), interpolation was required to achieve the desired accuracy. Correction of values to *in-situ* pressure was also required. The sound-channel charts were based on the analysis of Russian pH contours by Lovett [25] while the CZ and surface charts were derived mainly from the Russian report.

In cases where there is no single clearly dominant mode, effective loss can be estimated by integrating over all ray paths using a pH profile. Five contour charts were provided for the selected depths 0, .5, 1, 2 and 4 km for this purpose. The GEOSECS [26] data have also been used to derive the 2 km contours in parts of the Pacific Ocean not covered by Russian work.

The estimation problem at higher latitudes differs in several respects because the thermocline disappears, making refraction uniformly upward. Water depths tend to be smaller also. Since details of pH variability nearer the surface are more important, a change in scale is indicated. PH contours in the World Ocean Atlas: Arctic Ocean Vol. 3 cover a depth range 0-3 km. Only the range 0-1 km is required for calculations.

$$A = A_1(MgSO_4) + A_2(B(OH)_3) + A_3(MgCO_3)$$

$$A_n = (S/35)\, a_n f^2 f_n / (f^2 + f_n^2)$$

$$a_1 = 0.5 \times 10^{-D(km)/20} \qquad f_1 = 50 \times 10^{T/60}$$

$$a_2 = 0.1 \times K \qquad f_2 = 0.9 \times 10^{T/70}$$

$$a_3 = 0.03 \times K \qquad f_3 = 4.5 \times 10^{T/30}$$

The pH parameter $K = 10^{(pH-8)}$ has been substituted in the global model formula above. Salinity dependence is taken as S/35, with the caveat that errors may be excessive outside the range 30-40 ppt. Temperature profiles can be derived from the SVP used in the computer code. Actually, they may not be required because the range is so small. Salinity variations appear to be negligible.

Figure 14 shows the rough outline of the 1 km depth contour. Propagation can be expected to be absorption-limited for ranges up to roughly 50 km in this region. In shallower waters outside the region, effects of the bottom can become significant and ranges are correspondingly less.

Figures 15 and 16 show surface contours of the K-factor for winter and summer, derived from pH contours in the World Ocean Atlas: Arctic Ocean. The complexity of the structure during warmer periods is probably due to melting and runoff. This variability should not affect absorption because the deeper portions of the ray paths are the most critical.

Figures 17-22 show the K-factor contours for all the depths given in the World Ocean Atlas: Arctic Ocean. Seasonal variations are expected to be much smaller at depths of 100m or greater and the structure appears to be relatively simple

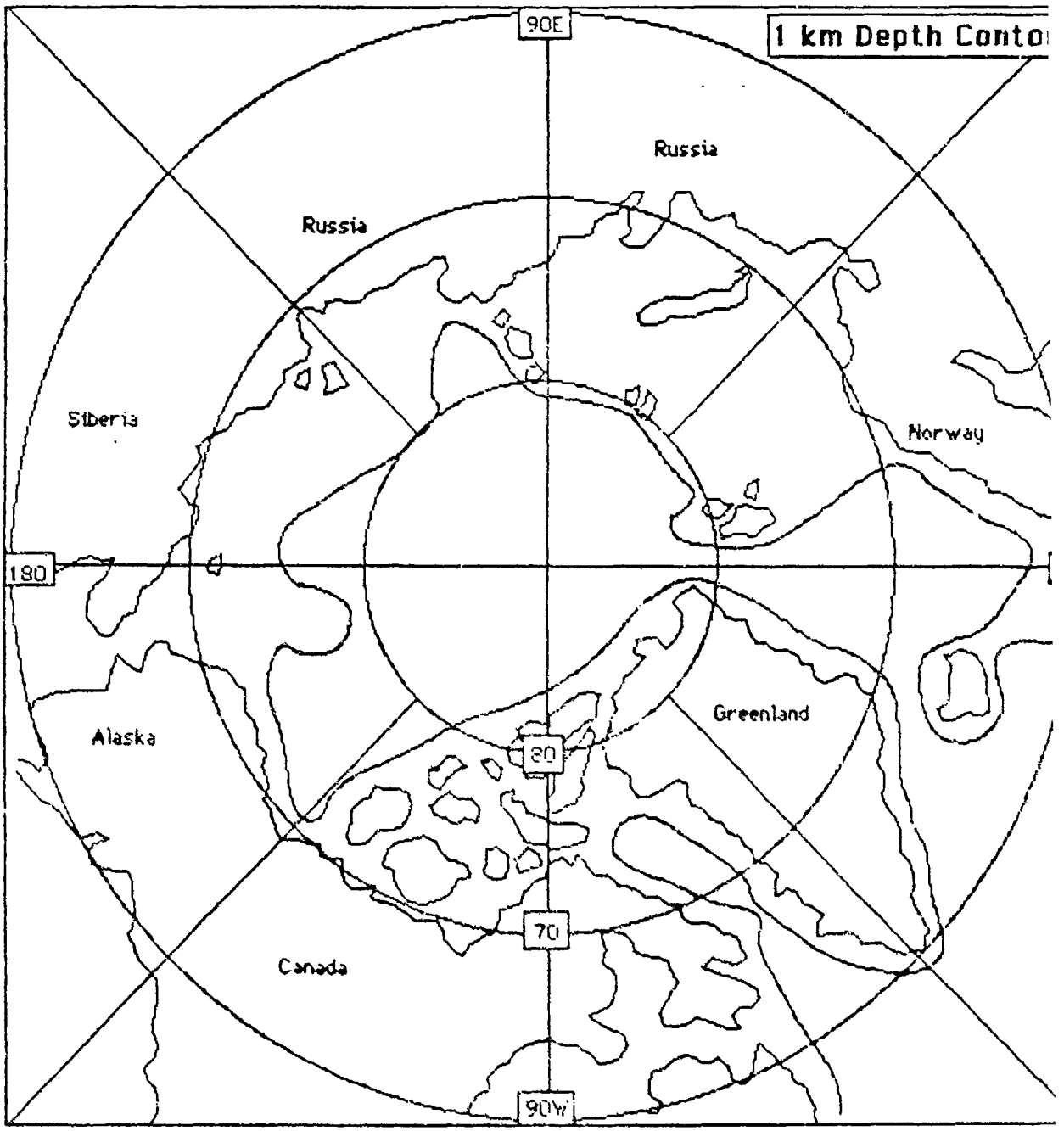

Figure 14. 1 km depth contour

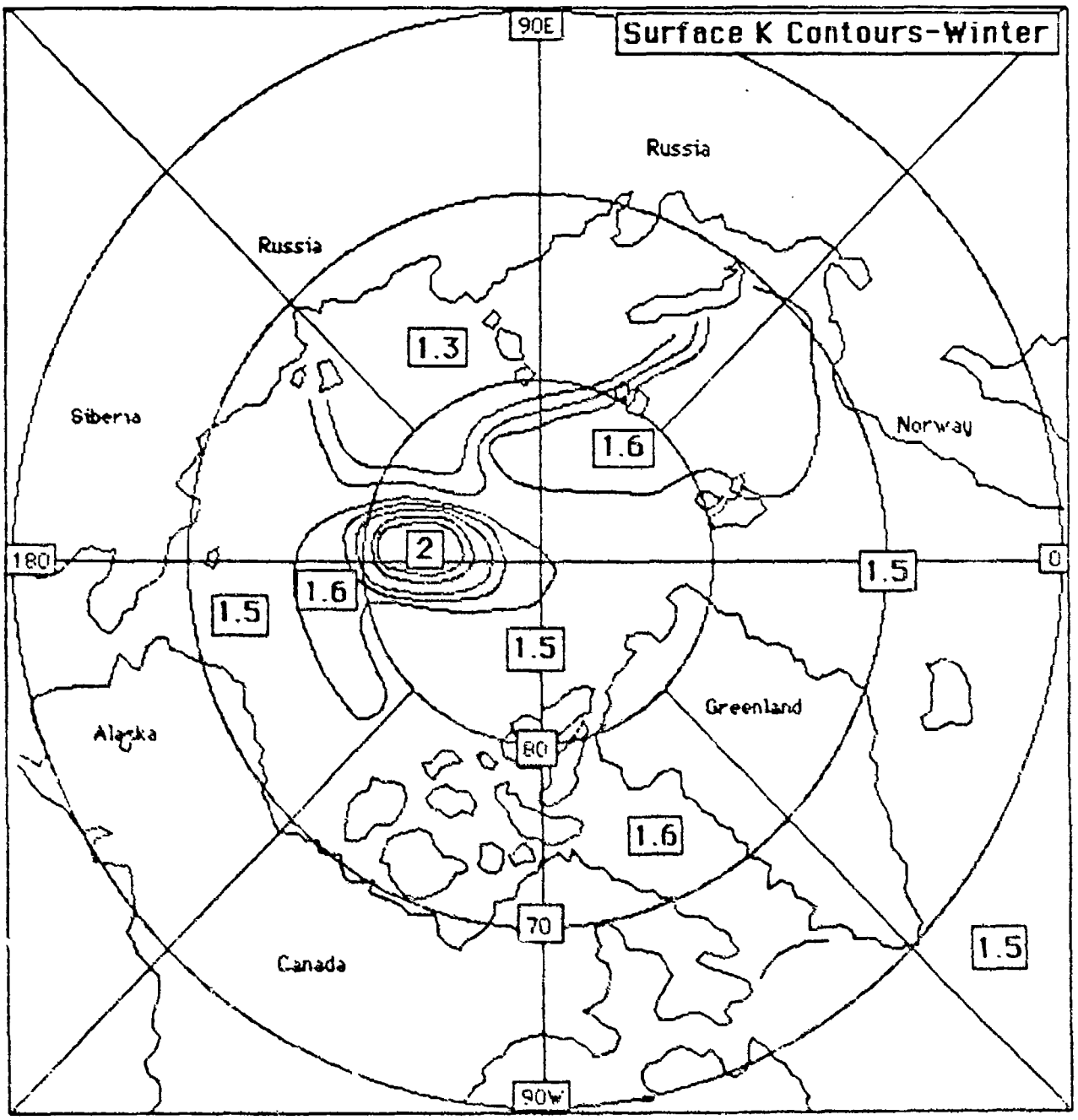

Figure 15 Surface K contours-winter

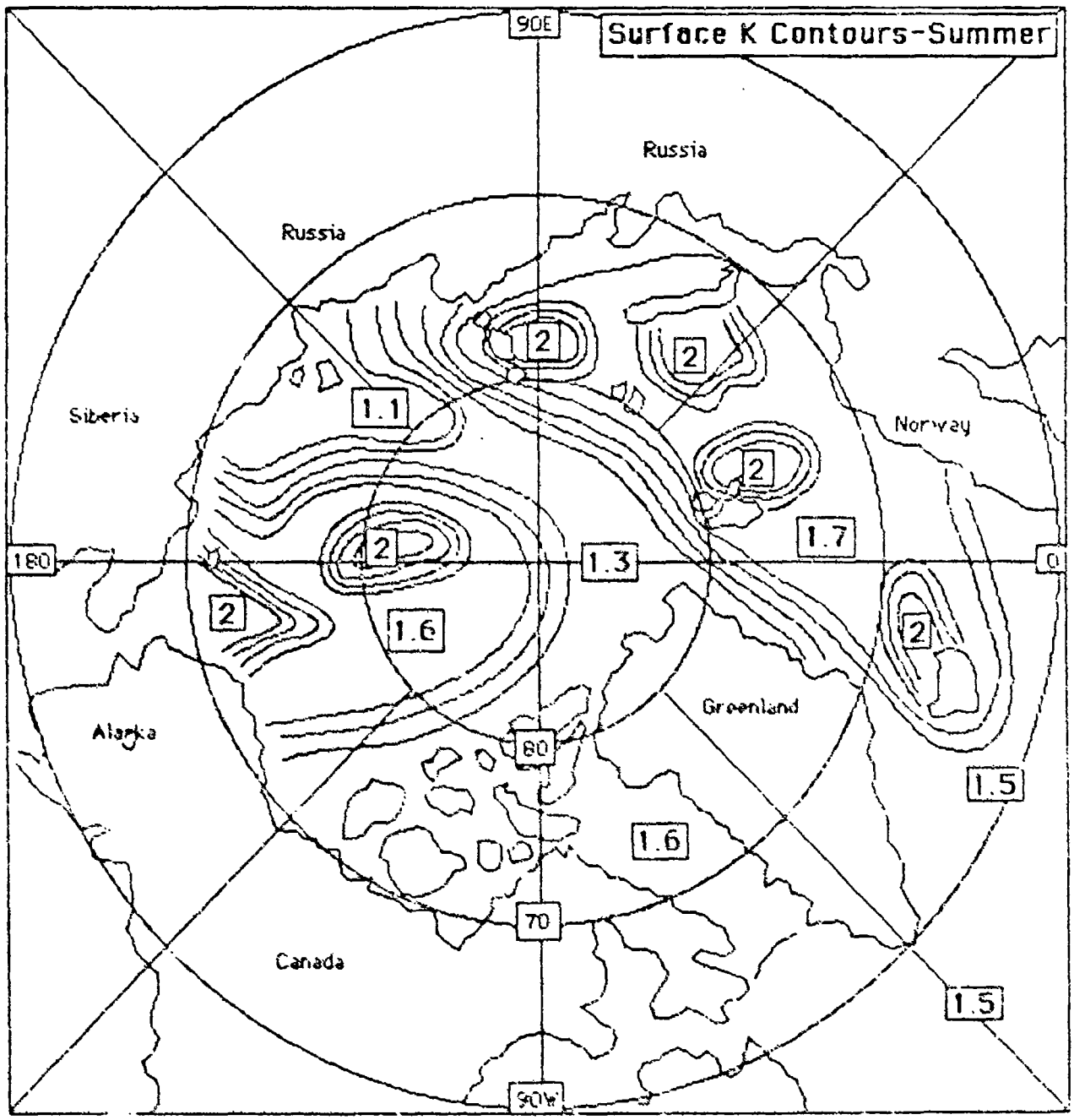

Figure 16. Surface K contours-summer

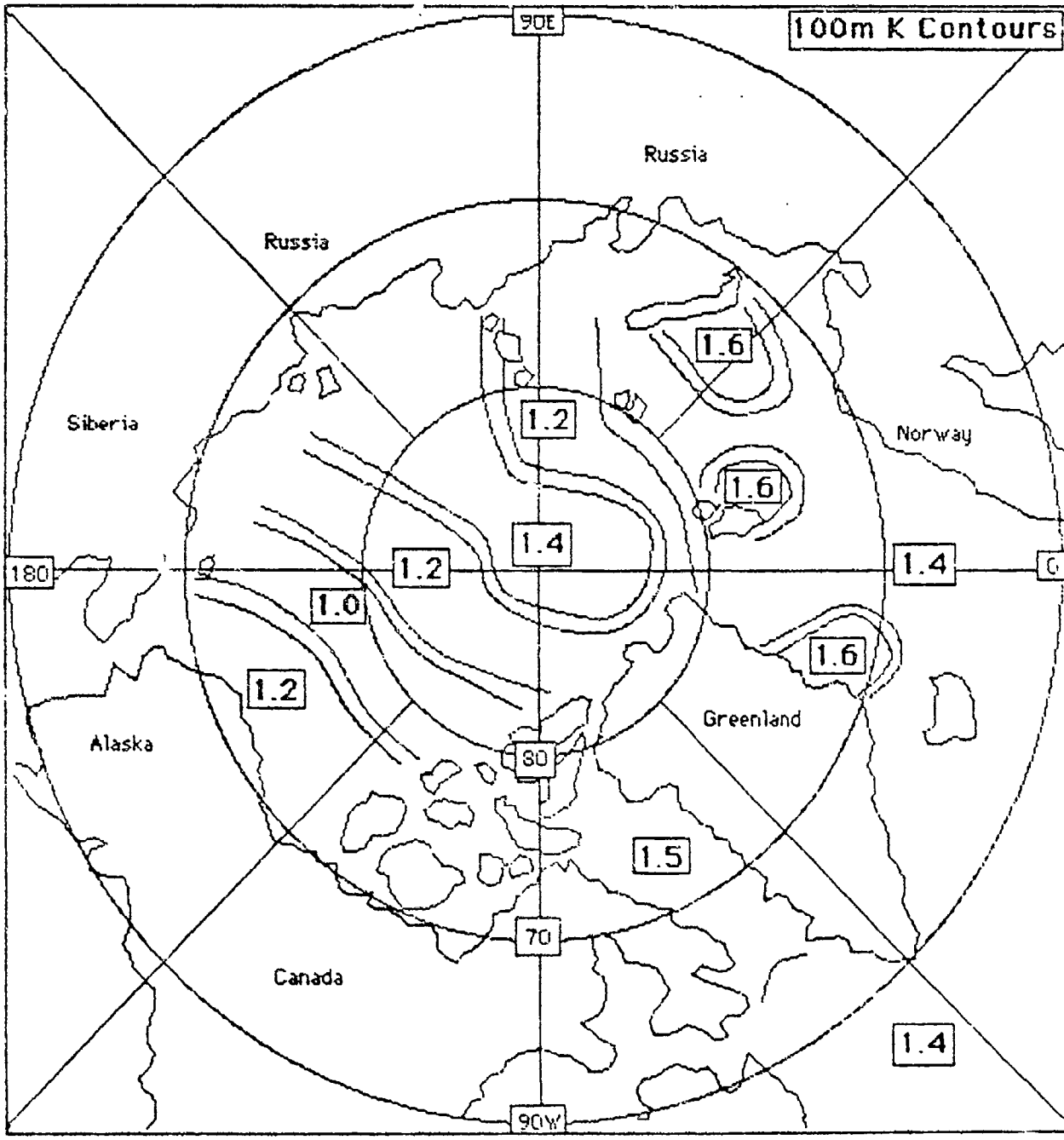

Figure 17 100m K contours

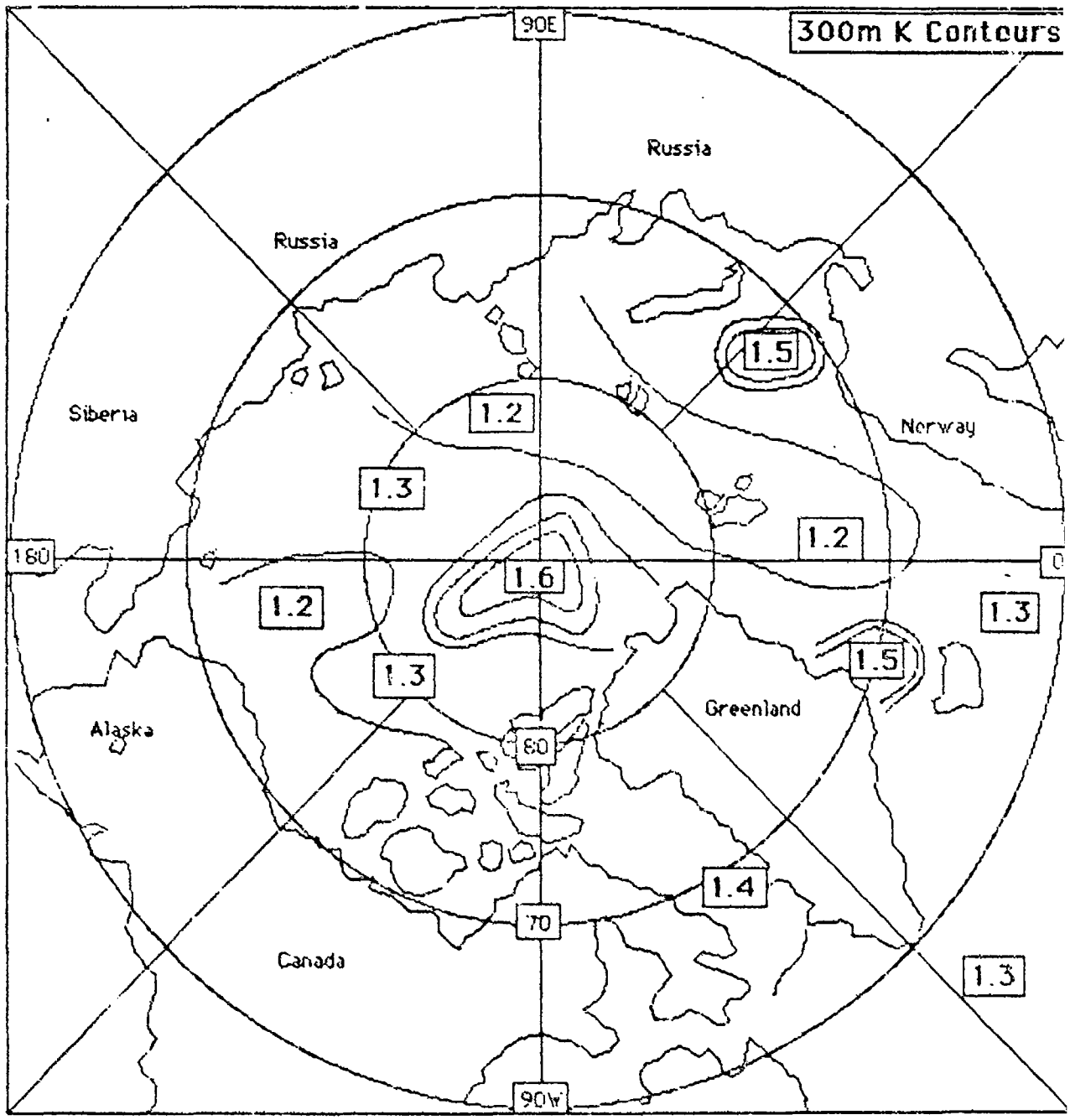

Figure 18 300m K contours

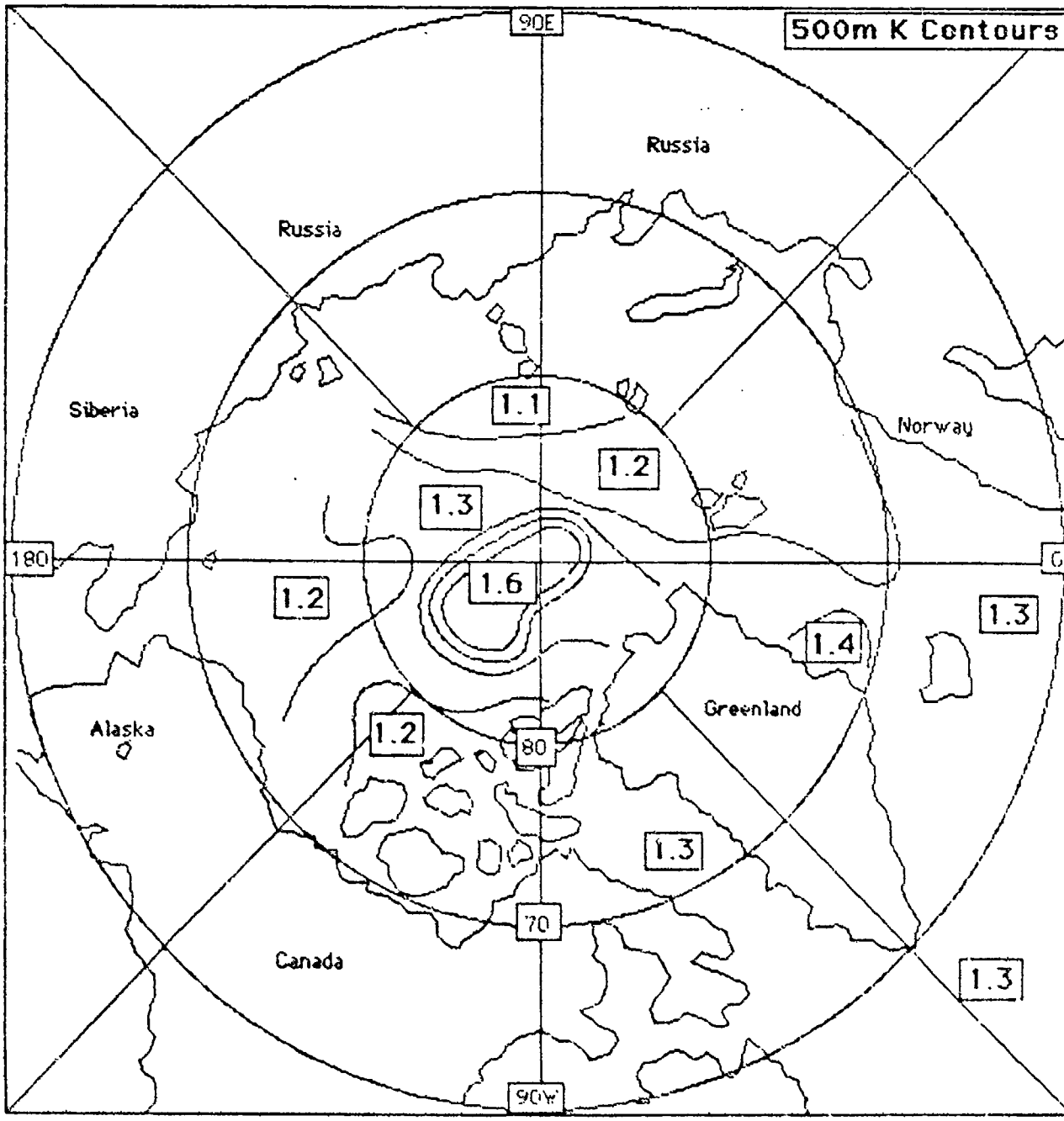

Figure 19 500m K contours

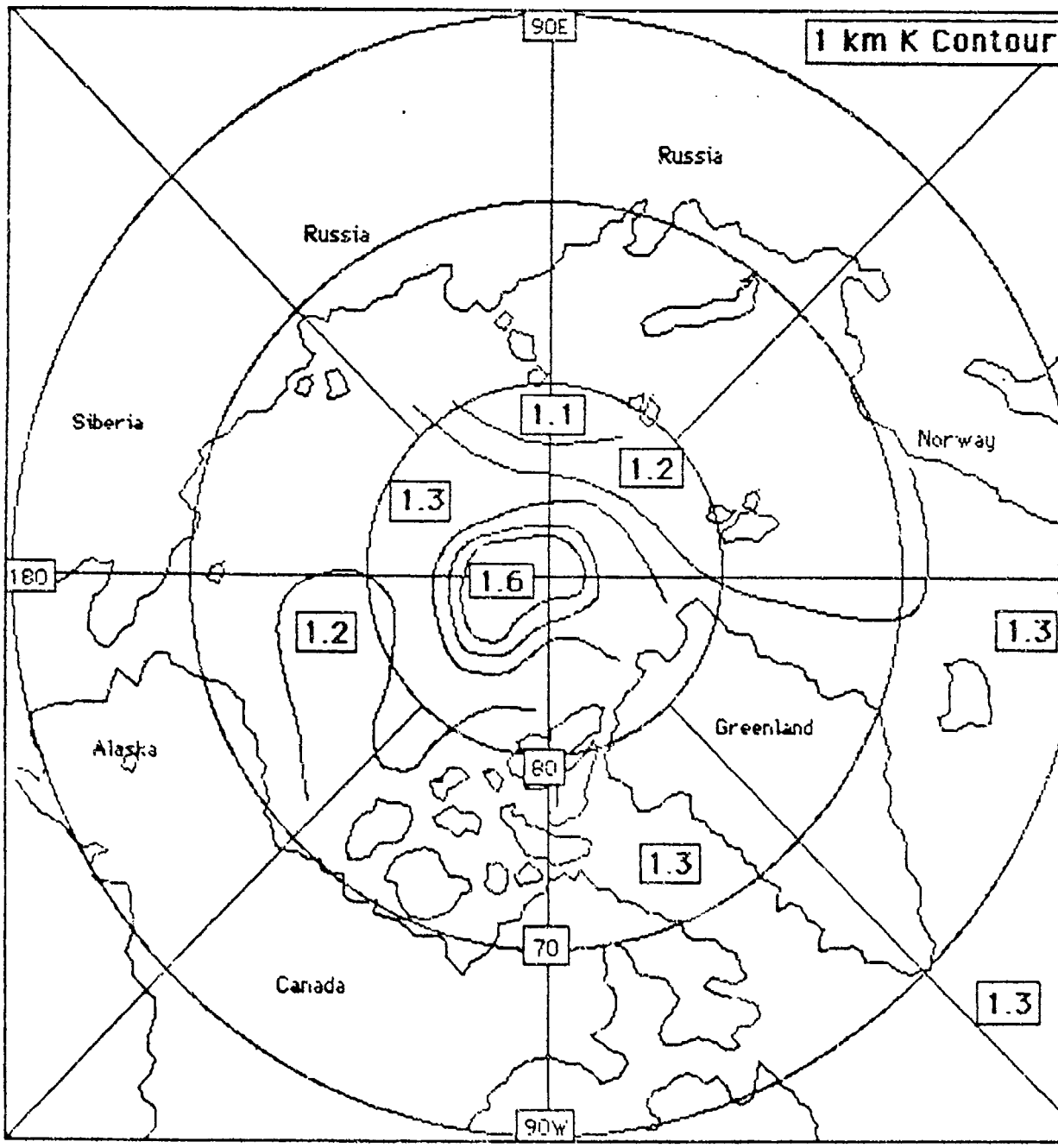

Figure 20: 1 km K contours

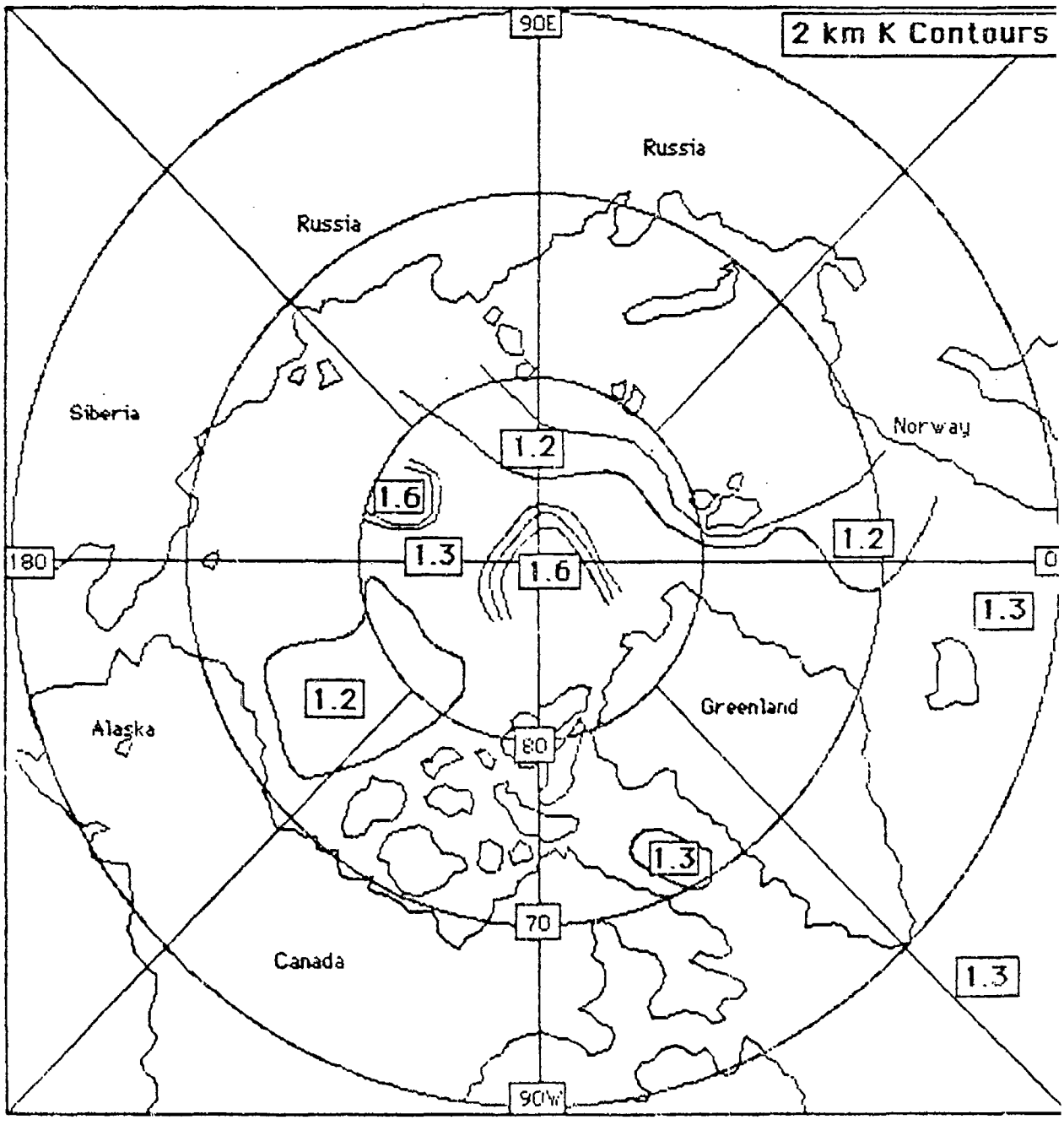

Figure 21. 2 km K contours

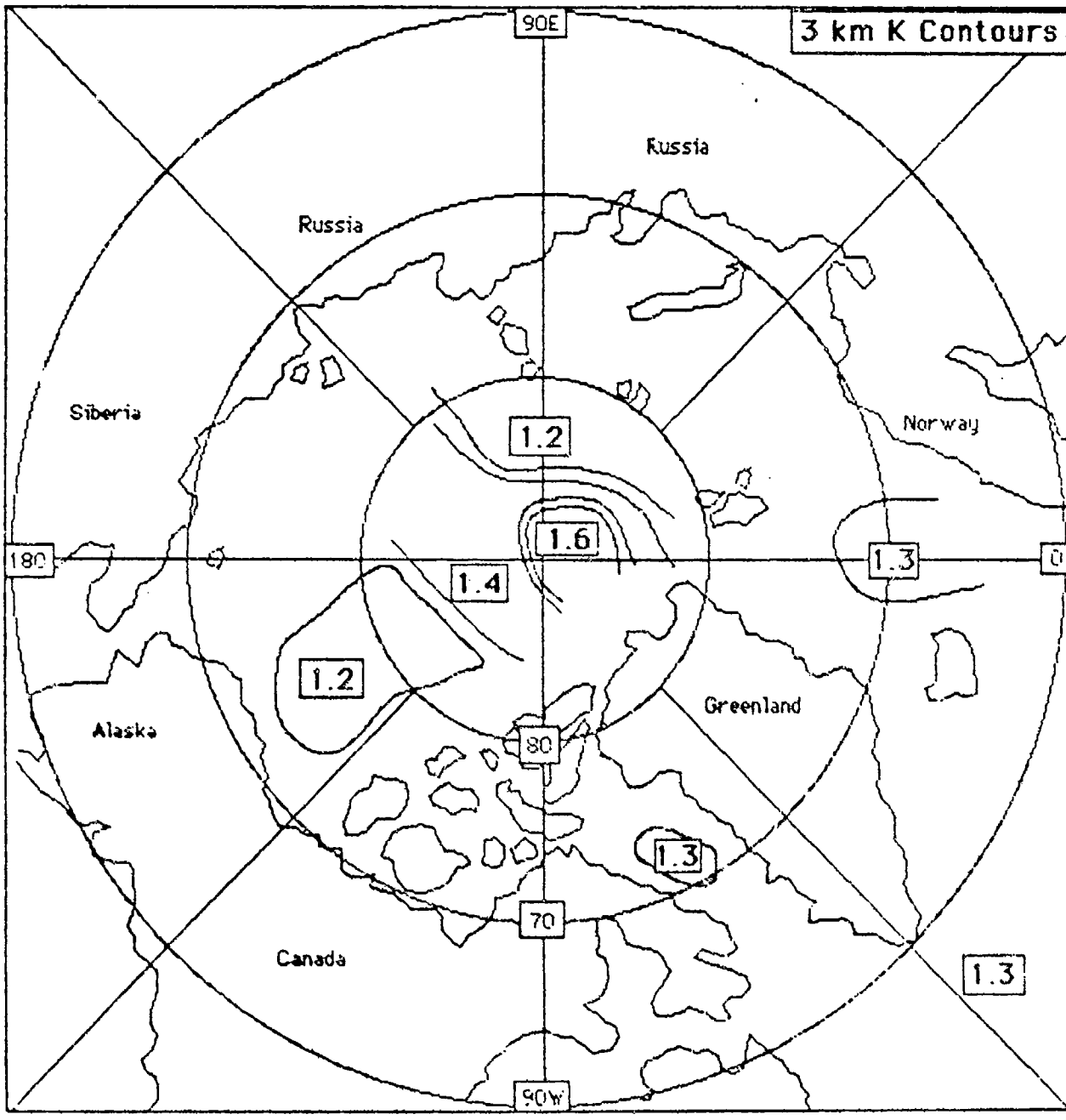

Figure 22. 3 km K contours

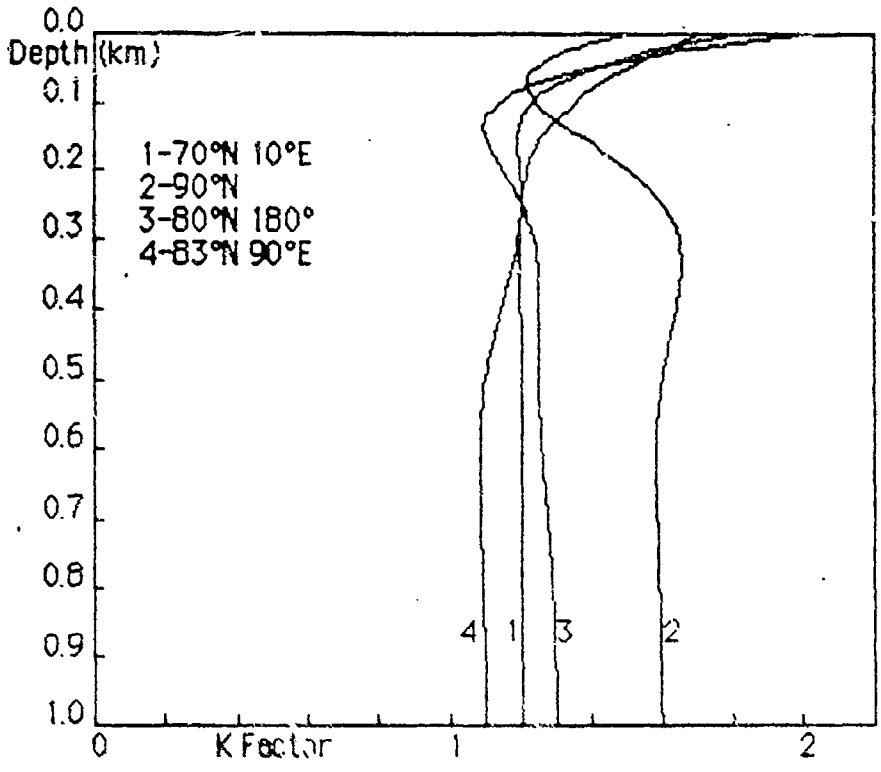

Figure 22: Arctic Ocean K-profiles.

The K-contour method has proven to give adequate accuracy in modeling the actual profiles throughout the World Ocean. The algorithm to be used again here was suggested by Dr. A. H. Nuttall.

The K values for D=0, 0.1, 0.3, 0.5, 1 km are labeled D_n where n=0,1,2,3,4. The profile is generated from the equation:

$$K(D)=K(D_4)+[C_0 + C_1 D + C_2 D^2 + C_3 D^3 + C_4 D^4] \exp[-(aD)^b]$$

where a=4/km and b=1.5 are found to give "best" results for Arctic regions. The five equations to be solved for the coefficients C_n are then given by:

$$C_0 + C_1 D_n + C_2 D_n^2 + C_3 D_n^3 + C_4 D_n^4 = [K(D_n) - K(D_4)] \exp[(4D_n)^{1.5}]$$

Either algebraic or matrix methods can be used.

Figure 22 shows typical profiles derived from the K-contour charts for several regions in the Arctic Ocean. The profiles appear quite consistent with the Russian data. Generally, the pH value is greatest at the surface and becomes constant at depths greater than about 0.5 km with a minimum near 0.1 km depth in some cases. The range of variation tends to be small compared to the World Ocean at lower latitudes [1,2].

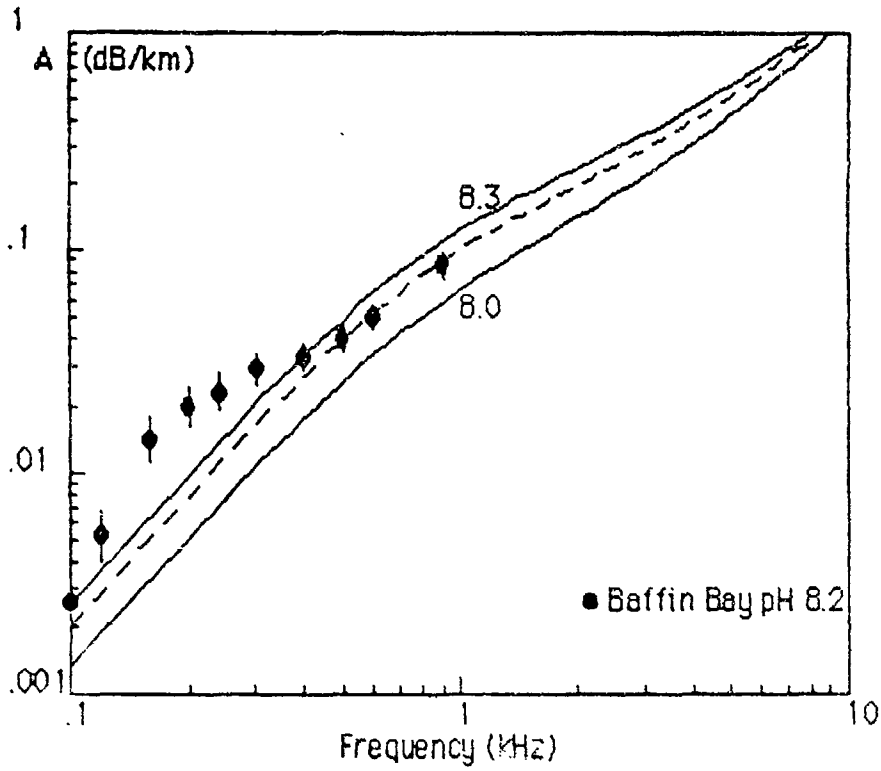

Figure 23: Absorption spectrum range in the Arctic.

Figure 23 shows the predicted range of variation of absorption spectra in the Arctic for the pH range 8.0-8.3 or K-factor range 1-2. Temperature is taken as -1°C and salinity as 35 ppt. Effects of pH below 10 kHz are due mainly to changes in the boric acid coefficient. At very low frequencies, the max/min ratio approaches the factor two. When compared to Atlantic spectra for pH=8.0, the range can exceed two because the temperature is higher.

The data points are from the Baffin Bay experiment of DREA [12 Vol.II]. These are the only available low-frequency Arctic data that clearly show the effects of the absorption limit. The experiment was carried out in the late summer under ice-free conditions. Near-surface temperatures were sufficiently high to form a weak thermocline and the propagation mode was sound-channel, the axis being near 100m in depth. The experimental range extended to roughly 400 km. The dashed curve for pH=8.2 (K≈1.6) gives the "best" data-fit at the higher frequencies.

The excess loss at the lower frequencies is probably due to scattering by temperature inhomogeneities in the medium, since neither ice or surface waves can be held responsible.

Model prediction comparison

2Alpha (dB)		70°N 10°E	90°N	80°N 180°	83°N 90°E
F (kHz)	R (km)>	40	40	40	40
45	K mod.	31.3	33.3	30.2	30.7
	Thorp	25.5	25.5	25.5	25.5
	Δ	5.8±0.6	7.8±0.6	4.7±0.6	5.2±0.6
40	K mod.	27.1	29.0	26.1	26.6
	Thorp	21.8	21.8	21.8	21.8
	Δ	5.3±0.6	7.2±0.6	4.3±0.6	4.8±0.6
3.5	K mod.	23.2	25.0	22.2	22.7
	Thorp	18.5	18.5	18.5	18.5
	Δ	4.7±0.5	6.5±0.5	3.8±0.5	4.3±0.5
3.0	K mod.	19.6	21.2	18.7	19.1
	Thorp	15.5	15.5	15.5	15.5
	Δ	4.1±0.5	5.7±0.5	3.2±0.5	3.6±0.5
2.5	K mod.	16.2	17.6	15.4	15.7
	Thorp	12.8	12.8	12.8	12.8
	Δ	3.3±0.4	4.8±0.4	2.5±0.4	2.9±0.4

Figure 24: Model comparison of 2.5-4.5 kHz two-way losses at 40 km.

In most cases, propagation in the high Arctic will be absorption-limited only for single refraction paths. The ranges of concern are therefore much shorter. Two-way loss predictions for the K model and the Thorp equation for the range 40 km are compared in Figure 24. The differences between the models, Δ=A(Kmod)-A(Thorp), also include the expected ± dB error of the K model, which indicates the degree of significance.

The ray-integration method and the algorithm profile were used in the K model calculations. Values of K at the five depths were fitted to generate the profiles. Salinity was taken as 35 ppt and temperature as -1°C. Losses at selected frequencies F(kHz) were calculated using the ray-integration method. Relative errors were calculated concurrently using the expected value ΔK=±0.05. The Thorp values were also calculated concurrently so as to minimize relative errors.

Figure 25 shows similar calculations for frequencies 5-9 kHz at 10 km range and for frequencies 10-18 kHz at 5 km range. Differences between models become negligible at the higher frequencies. Results above 10 kHz are in very good agreement with reported experimental values [27].

2Alpha (dB)		70°N 10°E	90°N	80°N 180°	83°N 90°E
F (kHz)	R (km)>	5	5	5	5
18	K mod.	30.5	29.9	30.5	30.4
	Thorp	31.1	31.1	31.1	31.1
	Δ	-0.6±0.1	-1.2±0.1	-0.6±0.1	-0.7±0.1
16	K mod.	25.3	24.7	25.3	25.2
	Thorp	25.2	25.2	25.2	25.2
	Δ	0.1±0.1	-0.4±0.1	0.2±0.1	0.0±0.1
14	K mod.	20.4	19.9	20.5	20.4
	Thorp	19.8	19.8	19.8	19.8
	Δ	0.7±0.1	0.1±0.1	0.7±0.1	0.6±0.1
12	K mod.	16.0	15.5	16.1	16.0
	Thorp	15.0	15.0	15.0	15.0
	Δ	1.1±0.1	0.6±0.1	1.1±0.1	1.0±0.1
10	K mod.	12.1	11.6	12.2	12.0
	Thorp	10.8	10.8	10.8	10.8
	Δ	1.3±0.1	0.8±0.1	1.4±0.1	1.3±0.1

2Alpha (dB)		70°N 10°E	90°N	80°N 180°	83°N 90°E
F (kHz)	R (km)>	10	10	10	10
9	K mod.	21.3	20.3	21.3	21.1
	Thorp	18.6	18.6	18.6	18.6
	Δ	2.7±0.2	1.7±0.2	2.7±0.2	2.5±0.2
8	K mod	18.0	17.0	17.9	17.8
	Thorp	15.2	15.2	15.2	15.2
	Δ	2.8±0.2	1.8±0.2	2.8±0.2	2.6±0.2
7	K mod	14.9	14.0	14.9	14.8
	Thorp	12.1	12.1	12.1	12.1
	Δ	2.8±0.2	1.9±0.2	2.8±0.2	2.6±0.2
6	K mod	12.2	11.3	12.1	12.0
	Thorp	9.5	9.5	9.5	9.5
	Δ	2.7±0.2	1.8±0.2	2.7±0.2	2.5±0.2
5	K mod	9.7	8.9	9.7	9.5
	Thorp	7.2	7.2	7.2	7.2
	Δ	2.5±0.2	1.7±0.2	2.5±0.2	2.3±0.2

Figure 25 Model comparison of 5-18 kHz two-way losses at 5 and 10 km.

Alpha (dB) SC		70°N 10°E	Atl. 30°N	Pac. 45°N	E. Med.
F (kHz)	R (km)>	200	200	200	200
2.0	K mod.	37.3	28.7	16.5	47.3
	Thorp	26.6	26.6	26.6	26.6
	Δ	10.7±1.0	2.2±1.0	-10.1±1.0	20.7±1.2
1.5	K mod.	28.5	21.6	11.7	35.3
	Thorp	20.4	20.4	20.4	20.4
	Δ	8.2±0.8	1.3±0.8	-8.7±0.8	14.9±0.9
1.0	K mod.	18.8	13.6	7.1	21.0
	Thorp	13.3	13.3	13.3	13.3
	Δ	5.4±0.6	0.2±0.5	-6.3±0.6	7.7±0.5
0.7	K mod.	12.0	8.2	4.3	12.1
	Thorp	8.4	8.4	8.4	8.4
	Δ	3.6±0.4	-0.2±0.3	-4.2±0.4	3.7±0.3
0.5	K mod.	7.2	4.7	2.5	6.7
	Thorp	5.0	5.0	5.0	5.0
	Δ	2.2±0.2	-0.3±0.2	-2.5±0.2	1.7±0.2

Figure 26: Model comparison of 0.5-2 kHz one-way losses at 200 km.

Ice-free conditions can exist in the Norwegian Sea during the summer months and propagation to very long ranges is possible at low sea-states. If the surface temperature rises enough to form a shallow sound-channel, refraction effects can make surface scattering negligible. However, the thermocline structure can still be "rough" and this evidently produces internal scattering. Excess losses may then occur a lower frequencies, like that observed in the Baffin Bay experiment

Figure 26 compares predicted one-way absorption loss for sound-channel propagation in the Norwegian Sea at 200 km range with other regions of the World Ocean. The full range of pH and temperature effects is realized only in these lower frequencies.

From the earlier analysis [1,2], absolute error of the absorption model is estimated to be less than ±15%, i.e. RMS error of the coefficient in dB/km is not expected to be greater than this if not limited by the accuracy of the environmental factors. Relative errors in estimating the effects of pH and temperature can be expected to be much smaller

Conclusion

The purpose of this effort has been to extend the global model for sound absorption in sea water [1,2] to cover Arctic regions. The method used in estimating sound absorption at lower latitudes appears equally effective in polar waters. The only modification required is the change in vertical scale. Since thermocline effects are absent, upward refraction dominates propagation and variations nearer the surface become more important. The depth range 0-1 km has therefore been selected for the K-contours and the scale of the K-profile algorithm changed from 1/km to 4/km.

The recommended method is numerical integration of losses over all ray paths by computer methods employing K-profiles. The five points from the K-contour charts should provide the required accuracy for the K-profiles. The algorithm method of generation is also recommended.

Temperature profiles can likewise be generated from the SVP used in the computer code. Since the nominal range is only -2°C to +4°C, effects will be small. The default value -1°C is suggested

Salinity variations fall in the range 32-35 ppt (except near the surface) and effects will also be minimal. The default value 35 ppt is suggested if local data are unavailable.

The K-profiles can, of course, be generated graphically; however, making a fit involves subjectivity and translation to a computer code is difficult. Linear interpolation would probably be more effective

A much simpler but less accurate method of estimating absorption is to select one K-value from the depth contour best suited to the propagation conditions in question. In deeper water, for example, the 0.5 km contours would probably be sufficiently accurate While the method is useful for rapid calculation, it is also more subjective

The final caveat is that no reliable data for polar waters appear to be available except for frequencies above 10 kHz Absorption predictions at the lower frequencies therefore rely solely on extrapolation of results obtained at higher temperatures Single-refraction path experiments in the range 1-10 kHz would help to resolve this problem. Excess losses observed at lower frequencies could involve some unknown absorption mechanism that becomes evident only at near-freezing temperatures Experiments using the resonator technique would serve as a method of investigating this possibility

References

1. R. H. Mellen, "Global model for sound absorption in sea water" PSI/MS Report #1412, Aug. 1986.
2. R. H. Mellen, "Global model for sound absorption in sea water: GEOSECS pH data analysis", PSI/MS Report #1310-83, Sept. 1986.
3. M. Schulkin and H. W. Marsh, "Sound absorption in sea water", J. Acoust Soc. Am. 34 864-865 (1962)
4. W. H. Thorp, "Deep ocean sound attenuation in the sub and low kilocycle-per-second region", J. Acoust. Soc. Am. 38, 648-654 (1965)
5. W. H. Thorp, "Analytic description of the low-frequency attenuation coefficient" J. Acoust. Soc. Am. 42 270-271 (1967)
6. C. C. Leroy, "Sound propagation in the Mediterranean Sea", in Underwater Acoustics, ed. V. M. Albers (Plenum, 1967) Vol. 2, pp. 203-241.
7. Attenuation of Low Frequency Sound in the Sea, Vol. I NUSC Scientific and Engineering Studies (1980)
8. R. H. Mellen and D. G. Browning, "Variability of low-frequency sound absorption: pH dependence", J. Acoust. Soc. Am. 61, 704-706 (1977)
9. E. Yeager, F. H. Fisher, J. Miceli and R. Bressel, "Origin of low-frequency sound absorption in sea water", J. Acoust. Soc. Am. 53, 1705-1707 (1973)
10. R. H. Mellen, D. G. Browning and V. P. Simmons, "Investigation of chemical sound absorption in sea water by the resonator method", J. Acoust. Soc Am Part I, 68, 248-257 (1980) Part II, 69, 1660-1662 (1981) Part III, 70, 143-146 (1981) Part IV, 74, 987-993 (1983)
11. R. H. Mellen, V. P. Simmons and D. G. Browning, "Sound absorption in sea water: a third chemical relaxation", J Acoust. Soc Am. 65, 923-925 (1974)
12. Attenuation of Low Frequency Sound in the Sea, Vol II NUSC Scientific and Engineering Studies (1981)
13. F. H. Fisher and V. P. Simmons, "Sound absorption in sea water", J Acoust Soc Am 62, 558-564 (1977)
14. R. H. Mellen and D. G. Browning, "Low-frequency sound absorption in the Pacific Ocean", J Acoust Soc Am 59 700-702 (1976)
15. R. H. Mellen, T. Akal, E. H. Hug and D. G. Browning, Low-frequency sound attenuation in the Mediterranean Sea", J Acoust. Soc Am 73 570 (1985)
16. Underwater Sound in the Arctic, NUSC Scientific and Engineering Studies (1984)

17. F. R. DiNapoli and R. H. Mellen, "Low-Frequency Attenuation in the Arctic Ocean", in Ocean Seismo-Acoustics , edited by T. Akal and J. M. Berkson, (Plenum Press, New York, 1986), pp. 387-395. Also NUSC Tech. memo. TM-851130, 1 Sept. 1985.
18 H. W. Marsh, M. Schulkin and S. G. Kneale, "Scattering of Underwater Sound by the Sea surface", J. Acoust. Soc. Am. 33, 334-340 (1961).
19. L. Brekhovskikh and Y. Lysanov, Fundementals of Ocean Acoustics, (Springer-Verlag, New York 1982), Ch. 9, Equation 9.6.6.
20. C. Ekart, "The Scattering of Sound from the Sea Surface", J. Acoust. Soc. Am. 25, 566-570 (1953).
21. H. W. Marsh, "Sound reflection and scattering from the sea surface" J. Acoust. Soc. Am. 35, 240-244 (1963).
22. B. F. Kur'yanov, "The scattering of sound at a rough surface with two types of irregularity", Sov. Phys. Acoust. 8, 252-257 (1963).
23. R. R. Greene and A. P. Stokes, "A model of acoustic backscatter from Arctic sea ice", J. Acoust. Soc. Am. 78 1699-1701 (1985)
24. World Ocean Atlas, edited by S. G. Gorshkov (Pergamon Press, New York)
Vol. 1, Pacific Ocean, pp.234-235 (1974)
Vol. 2, Atlantic and Indian Oceans, pp234-235 (1976)
Vol. 3, Arctic Ocean, pp.156-157 (1983)
25. J. R. Lovett, "Geographic variation of low-frequency sound absorption in the Atlantic, Indian and Pacific Oceans", J. Acoust. Soc. Am. 67 338-340 (1980)
26. GEOSECS Atlas, International Decade of Ocean Exploration (IDOE), Published by National Science Foundation (1981)
Vol. 1, Atlantic Expediton 1972-1973
Vol 3, Pacific Expedition 1973-1974
Vol. 5, Indian Ocean Expedition 1977-1978
27 R. E Francois and G R Garrison, "Sound absorption based on ocean measurements Part I: Pure water and magnesium sulfate contributions" J Acoust. Soc. Am. 72 896-907 (1982)

EXTERNAL DISTRIBUTION LIST

Addressee	No. of Copies
CINCLANTFLT	1
CINPACFLT	1
COMMANDER SECOND FLT	1
COMMANDER THIRD FLT	1
SURF FORCE LANT	1
SURF FORCE PAC	1
SUB FORCE LANT (CDR Callahan)	1
SUB FORCE PAC (Staff Oceanographer)	1
TRAINING COMMAND LANT	1
TRAINING COMMAND PAC	1
SUBMARINE GROUP 2 (LT Arango)	1
SUBMARINE GROUP 6 (CDR Dantzler)	1
SUBMARINE DEV GROUP 1	1
SUBMARINE DEV SQUADRON 12 (CDR W. Stephenson)	2
DEFENSE TECH INFO CENTER	1
CNO - NOP-095, NOP-951, NOP-952, NOP-953, NOP-098 NOP-981, NOP-987, NOP-02, NOP-21, NOP-22, NOP-03, NOP-62	12
CNR - OCNR-00, OCNR-10, OCNR-11, OCNR-12, OCNR-122, OCNR-124, OCRN-125, OCNR-127, OCNR-13, OCNR-20	10
OFFICE OF NAVAL RESEARCH DETACHMENTS	1
ONR DET BAY ST. LOUIS	1
ONR DET BOSTON	1
ONR DET PASADENA	1
NAIR-03	1
SPAWAR-00, PDW-124, SPAWAR-05	3
SEA-62, SEA-63	2
NRL	2
NRL DET CHESAPEAKE	2
NRL UND SOUND REF DET ORLANDO	2
NRL SPEC PROJ DET PT. MUGU	2
NORDA	2
NEPRF	2
NADC	2
NCSC (Ms. A. Bagnell)	2
NOSC	2
NOSC DET HAWAII	2
NPRDC	2
DTNSRDC	2
DTNSRDC CARDEROCK LAB	1
DTNSRDC ANNAPOLIS LAB	1
DTNSRDC ACOUS RES DET BAYVIEW	1
DTNSRDC DET BREMERTON	1
NUSC	1
NUSC NEWPORT LAB	4
NUSC NEW LONDON LAB	2
NUSC DET AUTEC	2
NUSC DET WEST PALM BEACH	2
NUSC DET TUDOR HILL	2
NUSC DET FT. LAUDERDALE	2
NUSC DET SENECA LAKE	2

EXTERNAL DISTRIBUTION LIST

Addressee	No. of Copies
NAVAL OCEANOGRAPHY COMMAND	2
NAVAL OCEANOGRAPHIC OFFICE	2
FLEET NUMERICAL OCEANOGRAPHY CTR	2
NTSA	1
NPS	1
NWC	1
SURF WARFARE OFFICERS SCHOOL COMMAND	1
SUBMARINE SCHOOL (Code 10, CDR Almon)	1
APPLIED PHYSIC LAB, JOHNS HOPKINS	1
APPLIED PHYSICS LAB, U. WASHINGTON	1
APPLIED RESEARCH LAB, PENN STATE	1
APPLIED RESEARCH LAB, U. TEXAS	1
MARINE PHYSICAL LABORATORY SCRIPPS	1
WOODS HOLE OCEANOGRAPHIC INSTITUTION	1
UNIV. OF CT, MARINE SCIENCES (Dr. F. W. Bohlen)	1
UNIV. OF NH, EARTH SCIENCES (Dr. F. Anderson)	1
UNIV. OF RI	1
PLANNING SYSTEMS INC (Dr. R. H. Mellen) Contract #N66604-87-M-B555	10